



Contents lists available at ScienceDirect

Metabolism

journal homepage: www.journals.elsevier.com/metabolism

The serine protease KLK7 promotes immune cell infiltration in visceral adipose tissue in obesity

Aleix Ribas-Latre^{a,b,c}, Anne Hoffmann^a, Claudia Gebhardt^a, Juliane Weiner^d, Lilli Arndt^e, Nora Raulien^e, Martin Gericke^e, Adhideb Ghosh^f, Kerstin Krause^{d,g}, Nora Klötting^a, Paul T. Pfluger^{g,h,i}, Bilal N. Sheikh^{a,d}, Thomas Ebert^d, Anke Tönjes^d, Michael Stumvoll^{a,d,g}, Christian Wolfrum^f, Matthias Blüher^{a,d,g}, Ulf Wagner^d, Joan Vendrell^{b,c,j}, Sonia Fernández-Veledo^{b,c,j}, John T. Heiker^{a,d,k,*}

^a Helmholtz Institute for Metabolic, Obesity and Vascular Research (HI-MAG) of the Helmholtz Zentrum München at the University of Leipzig and University Hospital Leipzig, Leipzig, Germany

^b Hospital Universitari Joan XXIII de Tarragona, Institut d'Investigació Sanitària Pere Virgili (IISPV), 43005 Tarragona, Spain

^c CIBER de Diabetes y Enfermedades Metabólicas Asociadas (CIBERDEM)-Instituto de Salud Carlos III (ISCIII), 28029 Madrid, Spain

^d Medical Department III - Endocrinology, Nephrology, Rheumatology, University of Leipzig Medical Center, Leipzig, Germany

^e Institute of Anatomy, Leipzig University, Leipzig, Germany

^f Laboratory of Translational Nutrition Biology, Institute of Food, Nutrition and Health, ETH Zürich, Schwerzenbach, Switzerland

^g German Center for Diabetes Research, Neuherberg, Germany

^h Research Unit NeuroBiology of Diabetes, Institute for Diabetes and Obesity, Helmholtz Centre, Munich, Germany

ⁱ Division of Neurobiology of Diabetes, TUM School of Medicine & Health, Technical University of Munich, Munich, Germany

^j Universitat Rovira i Virgili (URV), 43201 Reus, Spain

^k Institute of Biochemistry, Faculty of Life Sciences, Leipzig University, Leipzig, Germany

ARTICLE INFO

Keywords:

Serpin
Protease
Metabolic disease
Obesity
Adipose tissue
Inflammation

ABSTRACT

Obesity is a major health problem associated with global metabolic dysfunction and increased inflammation. It is thus critical to identify the mechanisms underlying the crosstalk between immune cells and adipose tissue that drive cardiovascular and metabolic dysfunction in obesity. Expression of the kallikrein-related serine protease 7 (KLK7) in adipose tissue is linked to inflammation and insulin resistance in high fat diet (HFD)-fed mice. Here, we engineered mice with a macrophage-specific KLK7 knockout (KLK7MKO) to investigate how KLK7 loss impacts immune cell function and obesity-related pathology. Compared to control mice, we observed lower levels of systemic inflammation, with less infiltration and activation of inflammatory macrophages in HFD-fed KLK7MKO mice, particularly in the epididymal adipose tissue. Mechanistically, we uncover that *Klk7* deficiency reduces pro-inflammatory gene expression in macrophages and restricts their migration through higher cell adhesion, hallmark features of macrophages in obese conditions. Importantly, through analyses of 1143 human visceral adipose tissue samples, we uncover that KLK7 expression is associated with pathways controlling cellular migration and inflammatory gene expression. In addition, serum KLK7 levels were strongly correlated with circulating inflammatory markers in a second cohort of 60 patients with obesity and diabetes. Our work uncovers the pro-inflammatory role of KLK7 in controlling inflammatory macrophage polarization and infiltration in visceral obesity, thereby contributing to metabolic disease. Thus, targeting KLK7 to control immune cell activation may dissociate adipose dysfunction from obesity, thereby representing an alternative obesity therapy.

1. Introduction

Over the past three decades, the world-wide prevalence of obesity

had tripled, prompting declarations of obesity an epidemic [1]. Obesity is a multifaceted condition influenced by various factors, including environmental, genetic, and psychosocial elements [2]. Despite

* Corresponding author at: Helmholtz Institute for Metabolic, Obesity and Vascular Research (HI-MAG) of the Helmholtz Zentrum München at the University of Leipzig and University Hospital Leipzig, Leipzig, Germany.

E-mail address: john.heiker@helmholtz-munich.de (J.T. Heiker).

<https://doi.org/10.1016/j.metabol.2025.156239>

Received 2 December 2024; Accepted 22 March 2025

Available online 26 March 2025

0026-0495/© 2025 The Authors. Published by Elsevier Inc. This is an open access article under the CC BY-NC-ND license (<http://creativecommons.org/licenses/by-nc-nd/4.0/>).

considerable research efforts to unravel the disease mechanisms underlying obesity, bariatric surgery, a high-risk procedure that severely alters the gut physiology, long remained the only long-term therapeutic option available for the most severe cases [3]. More recently, significant breakthrough was achieved in obesity pharmacotherapy through the development of incretin-mimetic drugs [4,5], although additional and endiology-based therapies are still required for unmet medical needs.

Obesity frequently leads to metabolic inflammation and adipocyte dysfunction, characterized by altered adipokine secretion and immune cell infiltration. These processes subsequently contribute to systemic inflammation, insulin resistance and the development of metabolic disorders [6]. Notably, in human obesity, inflammation in the adipose tissue (AT) and metabolic disease has been linked to an imbalance between proteases and their specific inhibitors [7–12]. Therefore, targeting proteolytic enzymes residing in AT may be a promising therapeutic approach to counteract AT inflammation in obesity. Consistently, inhibition of proteases in obese mice has been shown to exert beneficial effects on metabolic health. Regulating the expression or activity of proteases such as elastase, through genetic manipulations (deletion or transgenic overexpression of specific inhibitors) or pharmacological inhibition was reported to protect against high-fat diet-induced weight gain, adipose tissue inflammation and insulin resistance in mice [12–17].

In the diet-induced obese mouse model, we and others have consistently found that overexpression of the serpin inhibitor vaspin (SERPINA12) in AT limits weight gain and adipose tissue inflammation while preserving insulin sensitivity [18,19]. In mechanistic studies, vaspin has been demonstrated to attenuate cytokine-induced inflammation in adipocytes and improve insulin sensitivity [20,21]. In recent work, we identified that kallikrein-related peptidase 7 (KLK7) is a serine protease inhibited by vaspin [22].

KLK7 is primarily expressed in skin and is a key player in the maintenance of the skin barrier function and desquamation [23,24]. Consistently, dysregulation of KLK7 as well as other KLK family members has been implicated in inflammatory skin conditions such as psoriasis, atopic dermatitis and Netherton's syndrome [25–28], and has also been implicated in cancer progression and autoimmune diseases [29]. Our recent work highlighted the role of KLK7 in metabolic regulation of AT in obesity. Specifically, we found that the inhibitory activity of vaspin is crucial for beneficial effects on glucose tolerance and insulin resistance in mice [22]. These effects are likely mediated by KLK7, which is co-expressed with vaspin in mouse pancreatic β -cells and able to specifically degrade insulin [22]. Notably, knockout of KLK7 had similar effects on metabolic health in diet-induced obese mice as overexpression of the serpin inhibitor vaspin. Specifically, mice with either adipose-specific or global KLK7 KO and fed a high-fat diet were found to have reduced body weight and fat mass gain [30,31]. Although the mice were still obese, AT inflammation was significantly reduced, concomitant with reduced hyperinsulinemia and increased insulin sensitivity, suggesting that KLK7 mechanistically impacts on AT inflammation and metabolic dysfunction in obesity [30,31].

However, functional roles of KLK7 in regulating immune cells, and specifically, potential effects on macrophages in obesity are unknown and remain unexplored. In this study, we show that KLK7 expression in macrophages drives AT inflammation in obesity by promoting inflammatory macrophage polarization as well as migration and infiltration of macrophages, particularly into the visceral AT in mice.

2. Methods

2.1. Animal studies

Mice were housed in a pathogen-free facility (3–5 mice per group and cage) at 23 °C on a 12 h light/dark cycle (unless stated otherwise) with ad libitum access to water and either standard chow (V1534, 9 % calories from fat, Ssniff®, Soest, Germany) or a high-fat diet (HFD;

E15772–34, 55 % calories from fat, Ssniff®, Germany) between the ages of 5–25 weeks. Using the Cre-lox system for conditional gene-targeting, we generated macrophage-specific *Klk7* knockout mice (KLK7MKO). We crossed C57BL6/NTac mice with conditional (floxed) *Klk7* alleles (*Klk7^{fllox/fllox}* by Taconic, Cologne, Germany; [30,31]) with mice expressing Cre-recombinase under control of the lysozyme 2 (*Lyz2*) promoter *LysM-Cre^{+/-}*, specific for myeloid cell lineage expression, to generate KLK7MKO (*Klk7^{fllox/fllox} LysM-Cre^{+/-}*) and wild type littermate controls, termed WT throughout the manuscript (*LysM-Cre^{+/-} Klk7^{fllox/fllox}* and *LysM-Cre^{-/-} Klk7^{fllox/fllox}*). In monocytes, granulocytes and mature macrophages, Cre-recombinase mediated the deletion of the floxed *Klk7* alleles. Mice were genotyped as previously described [31] and sacrificed at the age of 25 weeks at which point organs were harvested, weighed (liver, subcutaneous inguinal (iWAT) and epididymal (eWAT) and brown (BAT)) and processed for cell isolation (as described in the “macrophage isolation” section, Supplementary methods), histological or biochemical analyses, or snap frozen in liquid nitrogen.

2.2. Phenotypic characterization

We studied fifteen to twenty male mice of each genotype (KLK7MKO and WT) from an age of 4 up to 24 weeks under chow and HFD conditions. We recorded body weight weekly, body composition (fat and chow-fed mass) at the age of 4, 10, 17 and 23 weeks in awake animals using an EchoMRI system (Echo Medical Systems, Houston, TX, USA). Intraperitoneal glucose (GTT) and insulin (ITT) tolerance tests were performed at an age of 22 and 24 weeks, respectively, as previously described [30,31]. Energy metabolism was analyzed by indirect calorimetry using CaloSys V2.1 metabolic chambers (TSE Systems, Bad Homburg, Germany) at an age of 24 weeks as previously described [31]. Data were recorded every 5 min for five days at 23 °C, and after two days of acclimatization, data of three full days were analyzed. Energy expenditure data were analyzed using ANCOVA with body weight as a covariate as previously described [32]. For fecal energy analysis, fecal pellets (~2 g) were collected from HFD-fed mice ($n = 5$ per genotype) and dried for several days at 65 °C before measuring energy content using a C200 Oxygen Bomb Calorimeter (IKA, Staufen, Germany).

2.3. ELISA

We used ELISA to analyze serum levels of insulin (Mouse Insulin ELISA, Mercodia, Uppsala, Sweden), C-peptide (Mouse C-peptide ELISA, ALPCO, Salem, USA), leptin (Mouse Leptin ELISA, Crystal Chem, Downers Grove, USA), adiponectin (Mouse Adiponectin ELISA, Adipogen, San Diego, USA), MCP1 (Mouse/rat CCL2/JE/MCP-1 Quantikine ELISA, R&D Systems, Minneapolis, USA), TNFA (#43904, BioLegend, San Diego, USA) and KLK7 (E03K0074, Bluegene, Shanghai, China) according to the manufacturer's protocols. MCP1 (#432704, from BioLegend, San Diego, USA) was measured in eWAT and iWAT lysates, conditioned media, as well as in bone marrow derived macrophages (BMDM) and supernatants thereof.

2.4. Proteomic profiling

Protein abundance in WAT lysates was measured using a proximity extension assay (PEA), namely the Target 48 Mouse Cytokine panel (v.934001, Olink Proteomics, Uppsala, Sweden). Details are provided in the Supplementary Methods.

2.5. Histological analyses

AT histology measurements of adipocyte size distributions as well as immunohistochemical analyses were performed as previously described [31]. For the smaller sized lipid droplets in brown adipocytes (10–60 μ m, or larger under HFD conditions [33]), BAT slides were analyzed using the Adiposoft (ImageJ-Fiji) software to determine lipid droplet

diameters [34]. All objects <10 μm were omitted from the subsequent analysis. Immunohistochemistry was done using rabbit anti-CD68 polyclonal antibody (MAB101141, R&D Systems), and HRP-conjugated anti-rabbit antibody (Dako EnvisionTM+; Dako, Jena, Germany) and images were taken using a Keyence BZ-X800 fluorescence microscope (Keyence, Osaka, Japan).

2.6. Macrophage isolation and culture

Adipose tissue macrophages (ATM) and bone marrow derived macrophages (BMDM) were isolated and cultured as described in [35,36]. Details are provided in the Supplementary Materials.

2.7. Analysis of mitochondrial respiration and mitochondrial content

BMDMs were seeded into 96-well Seahorse assay plates at 50,000 cells per well and assays were performed as published with minor modifications [37]. Macrophages were washed and incubated in assay medium (10 mM glucose, 2 mM L-glutamine, 1 mM sodium pyruvate in Seahorse XF base medium at pH 7.4) for 45–60 min at 37 °C (without CO₂). For mitochondrial stress tests, OCR and ECAR were measured in a Seahorse XFe96 analyzer after the following injections: 2 μM Oligo, 1 μM FCCP, and 0.83 μM Rot/AA (103015–100, Agilent). Data were normalized for cell content ratio of each well using the CyQUANT[®] Cell Proliferation Assay Kit (C7026) following the manufacturer's instructions and analyzed using the Wave software. To assess mitochondrial content, DNA was extracted using the Allprep[®] DNA/RNA Kit (Qiagen, Hilden, Germany) and a specific region of mtDNA (non-NUMT) was amplified in a qPCR reaction. The nuclear gene *B2m* was used for normalization.

2.8. RNA preparation and quantitative real-time-PCR (qPCR)

RNA isolation from tissues (adipose tissue, liver and skin) and macrophages (ATM, BMDM) was done using the Trizol protocol. qPCR was performed using the LightCycler System LC480 and LightCycler-DNA Master SYBR Green I Kit (Roche). Gene expression was calculated by the $\Delta\Delta\text{CT}$ method and normalized to *36b4* levels in each sample, as indicated. Primer sequences are listed in Supplementary table 1.

2.9. Preparation of eWAT conditioned medium

Epididymal WAT was dissected from four male WT or KLK7MKO mice fed a HFD for 20 weeks. Fat pads (average weight of 2517 \pm 569 mg) were minced into 2–3 mm³ fragments, pooled and incubated in DMEM (200 mg AT / ml) for 24 h in BioLiteTM 150 mm cell culture dishes (Thermo Scientific). Then, fresh DMEM was added for additional 24 h (final 100 mg AT/ml). Conditioned media (CM) were sterile filtered and stored at –80 °C until used. One lot of CM was used for all experiments and aliquots did not undergo multiple freeze and thaw cycles.

2.10. Cellular migration

BMDM migration capacity was measured using transwell inserts, for a 24 well plate, with a pore size of 8 μm (Costar, Corning, NY). In brief, BMDM (1 \times 10⁵ cells in 100 mL) from chow-fed and HFD-fed WT and KLK7MKO mice were seeded into the upper chamber of the insert and left to rest overnight under sterile conditions. The following day, the growth media was changed into serum-free medium and 600 μL of DMEM (non-stimulated conditions) or serum-free conditioned medium (CM – stimulated conditions), was loaded into the lower chamber. After incubation at 37 °C with 5 % CO₂ for 6 h, the BMDM were rinsed with PBS and non-migrated cells removed from the inserts using a cotton tip. Inserts were then fixed in 4 % formalin for 1 h and stained with DAPI for 15 min. The cells that had migrated to the lower surface of the membrane were counted in the whole area using the Image J software and the stitching function available in the Keyence BZ-X800 fluorescence

microscope. The number of migrated cells under stimulated conditions was expressed as a ratio relative to the number of cells that migrated under unstimulated conditions.

2.11. Electric cell-substrate impedance sensing (ECIS) measurements

ECIS plates (96W1E+; Applied Biophysics) were cleaned and stabilized overnight with 200 μL of DMEM per well at 37 °C. Wells were washed once with fresh PBS before seeding BMDM from HFD-fed WT or KLK7MKO mice at a density of 100,000 cells per well in 200 μL . Continuous impedance measurements were performed at 37 °C and 5 % CO₂ using an ECIS Z Θ instrument (Applied Biophysics) and resistance of the monolayer was calculated using the ECIS software [38].

2.12. Cell proliferation and ROS assays

To quantify cell proliferation, BMDM were incubated for 24h with EdU, scraped, and washed with PBS. Cells were fixed in 4 % formaldehyde (diluted in PBS) and directly labeled using the Click-iT[®] EdU Alexa Fluor 647 kit (C10424, Invitrogen) following manufacturer instructions. Samples were analyzed by cell cytometry, counting 50,000 events using a low flow rate during acquisition and Click-iT[®] EdU labeling was detected using logarithmic amplification of 650/660 nm excitation and a red emission filter. Raw data were processed using FlowJo software (Tree Star, Ashland, OR, USA). ROS levels in differentiated BMDM were measured using a standard assay (ab139476, Abcam).

2.13. Human data

2.13.1. Human data

2.13.1.1. Leipzig Obesity BioBank (LOBB) cohorts. The Leipzig Obesity BioBank (LOBB; <https://www.helmholtz-munich.de/en/hi-mag/cohort/leipzig-obesity-bio-bank-lobb>) comprises biomaterial including serum, plasma, adipose tissue, and other tissues, from donors with a wide range of data clinically relevant to obesity research. For these analyses, we included a consecutively recruited cross-sectional cohort of 1143 patients with obesity (women: $n = 813$; men: $n = 330$; mean \pm standard deviation: age = 46.8 \pm 11.8 years, BMI = 49.1 \pm 8.4 kg/m²; glucose metabolism characteristics – normal glucose tolerance (NGT): $n = 595$, impaired fasting glucose (IFG): $n = 25$, impaired glucose tolerance (IGT): $n = 40$, type 2 diabetes (T2D): $n = 483$) and 26 patients without obesity (women: $n = 14$; men: $n = 12$; age = 58 \pm 13.3 years, BMI = 25.8 \pm 2.5 kg/m²; diabetes state – no: $n = 23$, type 2 diabetes (T2D): $n = 3$). IFG, IGT and T2D were defined according to the criteria of the American Diabetes Association (ADA) in “Standards of Medical Care in Diabetes” [39]. Samples of intra-abdominal omental visceral (VIS) and abdominal subcutaneous (SC) adipose tissue fat depots (~1–2 g per biopsy) were collected during elective laparoscopic surgery between 2008 and 2018 at predefined locations, following standardized protocols [40,41] to ensure uniform biosampling. Simultaneously, measurements of body composition and metabolic parameters were obtained according to standardized and previously published protocols [42]. The biobanking was carried out at the University Hospital of Leipzig Obesity Center using a validated storage system. The biobank stores various materials in different forms (DNA, RNA, cells, fluids) at different temperatures (–80 °C and –130 °C). Exclusion criteria encompassed participants under 18 years of age, chronic substance, or alcohol misuse, smoking within the 12 months prior to surgery, acute inflammatory diseases, use of glitazones as concomitant medication, end-stage malignant diseases, weight loss exceeding 3 % in the three months preceding surgery, uncontrolled thyroid disorder, and Cushing's disease.

2.13.1.2. Leipzig endocrinology cohort. The design of this cross-sectional

study has been described recently [43,44]. Here, $n = 60$ adults (women: $n = 33$; men: $n = 27$; mean \pm standard deviation: age = 62.5 ± 10.4 years, BMI = 30.2 ± 5.5 kg/m²) were recruited by the Department of Endocrinology and Nephrology, University of Leipzig. 50 % of the patients had a diagnosis of T2D. Inclusion criteria were subjects >18 years of age and written informed consent. Exclusion criteria were end-stage malignant diseases, pregnancy, acute generalized inflammation, acute infectious disease, and history of drug abuse.

2.14. Bulk RNA sequencing and analysis

RNA was extracted from subcutaneous (SC) and visceral (VIS) adipose tissue samples obtained from each participant of the LOBB cohort using the SMARTseq protocol [45,46]. The RNA was enriched and reverse-transcribed using Oligo(dT) and TSO primers, followed by cDNA amplification with PCR primers that were *in-silico* tested. cDNA was processed using a Nextera DNA Flex kit with Tn5 transposase. Single-end sequencing of all libraries was conducted on a Novaseq 6000 instrument at the Functional Genomics Center in Zurich. Raw sequencing reads underwent adapter and quality trimming using Fastp (v0.20.0, [47]), with a minimum read length of 18 nucleotides and a quality cut-off of 20. Read alignment against the human reference genome (assembly GRCh38.p13, GENCODE release 32, [48]) and gene-level expression quantification were performed using Kallisto (v0.48, [49]). Samples with read counts exceeding 20 million were downsampled to 20 million read counts using the R package ezRun (v3.14.1; <https://github.com/uzh/ezRun>, accessed on 23 March 2022). The data were normalized using a weighted trimmed mean (TMM) of the log expression ratios [50]. Batch effects were explored using the R swamp package (v1.5.1; <https://CRAN.R-project.org/package=swamp>, accessed on 23 March 2022) and adjusted using limma (v3.56.2, [51]). The data were adjusted for age and sex.

2.15. Gene set enrichment analyses

To predict the gene function of KLK7 and identify potential associations with Kyoto Encyclopedia of Genes and Genomes (KEGG) pathways [52], we conducted Gene Set Enrichment Analysis (GSEA, [53]) of the RNA sequencing data of the LOBB cohort using the R package CorrelationAnalyzer (v1.0.0; [54]). We then performed GSEA annotations for KLK7 by considering co-expression correlations with other genes within the cross-sectional LOBB cohort for both VIS and SC AT RNA-seq datasets applying the single gene mode of the correlationAnalyzer R package. In this analysis, genome-wide Pearson correlations were employed as a pre-ranking metric for the GSEA algorithm. To address the issue of multiple testing, we corrected the analyses using the false discovery rate (FDR) method.

2.16. Serum targeted biomarker analysis

In all individuals of the Leipzig Endocrinology cohort, blood samples were taken after an overnight fast. Using Proximity Extension Assay technology, the Olink Target 96 (v3021) Inflammation panel was measured in serum by real-time polymerase chain reaction (PCR) on the Fluidigm BioMark HD real-time PCR platform according to the manufacturer's protocol (Olink, Uppsala, Sweden). After intensity normalization (v2) and transformation, data are expressed as NPX. Proteins measurements below the LOD in >50 % of the samples from each group were excluded ($n = 10$). The remaining low expression values (NPX < LOD) were replaced by LOD/ $\sqrt{2}$ to obtain a conservative estimate for the low values that are below the detection limit. Negative expression values were retained. In total, 82 quantified proteins were used for downstream analysis. KLK7 in serum was measured via the human Kallikrein 7/KLK7 ELISA Kit (ab287175, abcam), according to the manufacturer's protocol.

2.17. PBMC isolation and KLK7 measurements

Blood was obtained from $n = 13$ donors in Tarragona (age = 52.84 ± 13.56) with ($n = 7$, BMI 33.20 ± 1.71) or without ($n = 6$, BMI = 22.95 ± 1.95) obesity. Human PBMCs were isolated using Ficoll-Hypaque gradients (Amersham Bioscience). Between $4\text{--}7 \times 10^6$ PBMCs were cultured using supplemented DMEM medium (10 % FBS), and incubated at 37 °C in a humidified, 5 % CO₂ atmosphere. After 3 days, the cells were washed with PBS to eliminate lymphocytes, and fresh media was added to the remaining attached cells (predominantly monocytes and macrophages). After 7 more days, the conditioned media was saved to measure KLK7 release according to manufacturer's protocol (ab287175, abcam).

2.18. Statistical analysis

If not stated otherwise, data are presented as means \pm SEM. For correlation heatmaps of the human data, univariate Spearman correlations were calculated using the R package RVAideMemoire (v0.9–81–2, <https://CRAN.R-project.org/package=RVAideMemoire>, accessed on 23 March 2022) and corrected for multiple inferences by considering the sample-size-appropriate false discovery rate (FDR). Bioinformatic analyses were carried out in R v4.3.1. All other statistical analyses were performed using GraphPad Prism 10 (GraphPad, San Diego, CA, USA). Methods of statistical analyses were chosen based on the design of each experiment and are indicated in the figure legends. Adjusted $p < 0.05$ were considered statistically significant.

2.19. Study approval

2.19.1. Animal studies

All animal experiments were approved by the local authorities of the Free State of Saxony (TVV11/20; TVV24/21; T09/21, Landesdirektion Leipzig, Germany), as recommended by the responsible local animal ethics review board.

2.19.2. Leipzig Obesity BioBank (LOBB) cohorts, Leipzig Endocrinology (LE) cohort, Tarragona cohort

Written informed consent was obtained from all patients. All studies were approved by the Ethics Committee of the University of Leipzig (LOBB approval numbers: 159–12–21,052,012 and 017–12ek; LE approval numbers: 140–2008 and 180/13–ff) or the Ethics and Research Committee of Institut d'Investigació Sanitària Pere Virgili (IISPV CEIm, Tarragona, Spain; approval number: CEIC 54c/2009) and performed in accordance with the Declaration of Helsinki, the Bioethics Convention (Oviedo), Good Clinical Practice Guidelines approved by the Health Department of Generalitat de Catalunya and EU Directive on Clinical Trials (Directive 2001/20/EC).

All serum and AT donors have been informed of the purpose, risks and benefits of the biobank. Ethical guidelines and EU legislation for privacy and confidentiality in personal data collection and processing is being followed, in particular directive 95/46/EC.

3. Results

3.1. Macrophage Klk7 expression is upregulated in obesity

To uncover how KLK7 expression is regulated in immune cells in obesity, we first investigated its expression in mouse macrophages derived from the bone marrow (BMDM). In HFD-fed mice, we found that *Klk7* expression was significantly elevated in BMDM ($p < 0.05$) (Fig. 1a). To test whether factors derived from AT were capable of increasing KLK7 expression in macrophages, we used an ex vivo approach. We tested whether conditioned medium (CM) from cultivated eWAT explants of HFD-fed mice would impact on KLK7 expression in BMDM (Fig. 1b). As expected, the expression of pro-inflammatory cytokines *Tnfa* and *Mcp1* was significantly induced in BMDMs after 6 h in CM

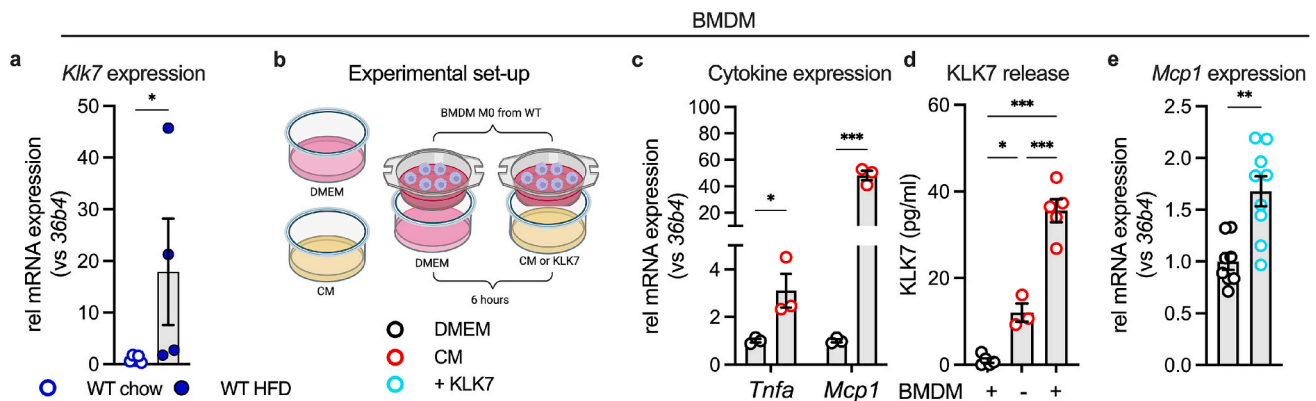


Fig. 1. *Klk7* expression in immune cells is significantly altered in obesity. a) RT-PCR analysis reveals higher expression of *Klk7* in bone marrow derived-macrophages (BMDM) isolated from HFD-fed (filled blue) when compared to chow-fed (outlined blue) wild type (WT) mice ($n = 4$). mRNA levels are relative to BMDM from chow-fed mice. b) Experimental set-up to assess the effect of conditioned media (CM) obtained from eWAT explants of HFD-fed WT mice, in cytokine expression (c) and KLK7 release (d) from BMDM isolated from chow-fed WT mice, after a period of six hours. c) RT-PCR analysis reveals significant induction of gene expression of *Tnfa* and *Mcp1* in CM-treated (red) BMDM compared to DMEM controls (black) ($n = 3$ per condition). mRNA levels are relative to controls. d) ELISA measurement reveals the presence of mouse KLK7 in CM (red -, $n = 3$) and further significant release of KLK7 from CM treated BMDM (red +, $n = 5$), compared to controls (DMEM, black, $n = 5$). Treatment was for 6 h without serum. e) RT-PCR analysis reveals higher *Mcp1* expression in BMDM from chow-fed WT mice treated with recombinant KLK7 over 24 h (turquoise, $n = 9$), compared to controls (black, $n = 8$). Significance ($p < 0.05$) was determined by unpaired two-tailed *t*-tests (a, e), multiple corrected unpaired two-tailed *t*-test (c) or by one-way ANOVA and Tukey's post-tests (d). (For interpretation of the references to colour in this figure legend, the reader is referred to the web version of this article.)

(Fig. 1c). Notably, CM-treated BMDMs released significantly more KLK7 into the supernatant compared to controls, with a substantial amount of KLK7 already present in the CM, i.e. released from the eWAT explant (Fig. 1d). To demonstrate direct effects of KLK7 on macrophage phenotypes, we ex vivo treated BMDM from WT mice with recombinant KLK7 for 24 h and found increased *Mcp1* expression (Fig. 1e).

Taken together, our data show that expression of *Klk7* in macrophages is elevated in diet-induced obese mice and acts through a paracrine mechanism to induce cytokine and KLK7 expression and secretion from BMDM.

3.2. Macrophage-specific deletion of *Klk7* ameliorates metabolic consequences of a high fat diet in mice

To delineate how KLK7 impacts on macrophage populations, we next generated mice with *Klk7* deficiency in myeloid cells. Specifically, we crossed mice carrying loxP-flanked *Klk7* alleles (*Klk7^{fllox/fllox}*) with mice expressing Cre-recombinase under control of the myeloid-specific lysozyme 2 (*Ly2*) promoter to specifically delete *Klk7* gene expression in macrophages (KLK7MKO) (Fig. 2a), as confirmed by qPCR (Fig. 2b). When fed a control chow diet, KLK7MKO mice were fertile and showed no differences in growth and development (Fig. 2c). However, after 20 weeks on HFD, KLK7MKO mice showed lower weight gain with reduced overall fat mass compared to WT mice (Fig. 2c-e, SF1a). Here, specifically the iWAT mass was lower, while eWAT and liver weights were not different in KLK7MKO mice compared to littermate controls (Fig. 2f). However, we did not find differences in food intake (Fig. 2g), energy expenditure (Fig. 2h), locomotor activity (SF1b), and respiratory exchange ratio (Fig. 2i) in KLK7MKO compared to littermate controls. Fecal energy contents were comparable between genotypes, excluding potential contributions of nutrient malabsorption due to alterations in gut immune cell landscape (Fig. 2j).

Lower inflammation may preserve the activity of thermogenic adipocytes in BAT or beige/browned WAT (BeAT) and this may contribute to the weight gain phenotype. While BAT mass was not different (SF1c), histology did show morphologic differences with less hypertrophic or whitened brown adipocytes (Fig. 2k) and a significantly lower percentage of large droplets $>60 \mu\text{m}$ in HFD-fed KLK7MKO mice (Fig. 2l). Among BAT marker genes, we found significantly higher *Ucp1* expression (Fig. 2m). Given the reduction of iWAT mass, we also measured

gene expression related to thermogenic BeAT (*Ucp1*, *Pgc1a*, *Tmem26*, *Serca2b*, *Ryr2*) but did not observe differences between genotypes (SF1d). Together, these data support improved or preserved BAT function in KLK7MKO mice.

Blood glucose levels in HFD-fed WT and KLK7MKO mice were higher compared to chow-fed mice, but not different (Fig. 3a). Similarly, glucose tolerance was affected by the HFD (Fig. 3b) but there were no genotype-specific differences. However, insulin tolerance tests (ITT) revealed significantly higher insulin sensitivity in KLK7MKO mice (Fig. 3c-e). To preclude major effects from overall lower body weight, the ITT were performed in mice selected for similar body weight and also fat mass (SF1e-f). A healthier metabolic phenotype of KLK7MKO mice was further reflected by a significantly improved profile of circulating markers of metabolic health. KLK7MKO mice had significantly lower serum KLK7 levels (Fig. 3f), indicating that immune cells are a significant source of circulating KLK7. Levels of pro-inflammatory cytokines TNFA and MCP1 were significantly lower in HFD-fed KLK7MKO mice (Fig. 3g-h), as were serum levels of leptin (Fig. 3i), which resulted in an improved leptin-to-adiponectin ratio (Fig. 3j-k). KLK7MKO also had lower insulin serum levels (Fig. 3l) and lower C-peptide levels (Fig. 3m) compared to WT mice, resulting in a higher insulin/c-peptide ratio (Fig. 3n). Together, our data show that HFD induces KLK7 expression in macrophages, which in turn accelerates the development of obesity, inflammation, and metabolic alterations. Consequently, genetic loss of KLK7 in myeloid cells mitigates the onset of these metabolic adaptations.

3.3. Obesity-induced immune cell infiltration and inflammation in epididymal white adipose tissue is mediated by KLK7

Next, we investigated WAT depots of HFD-fed KLK7MKO and control mice in greater detail. In line with increased *Mcp1* expression in BMDM treated with KLK7, release of MCP1 was significantly lower in BMDM derived from HFD-fed KLK7MKO relative to BMDM derived from WT controls (Fig. 4a). WAT levels of MCP1 in general were higher in eWAT compared to iWAT, but eWAT MCP1 was significantly lower in KLK7MKO (Fig. 4b). Consistently, targeted proteomic analysis of inflammatory cytokine abundances in WAT lysates confirmed an overall significantly lower inflammatory milieu in eWAT of KLK7MKO mice (Fig. 4c), while there were only subtle differences in the iWAT between

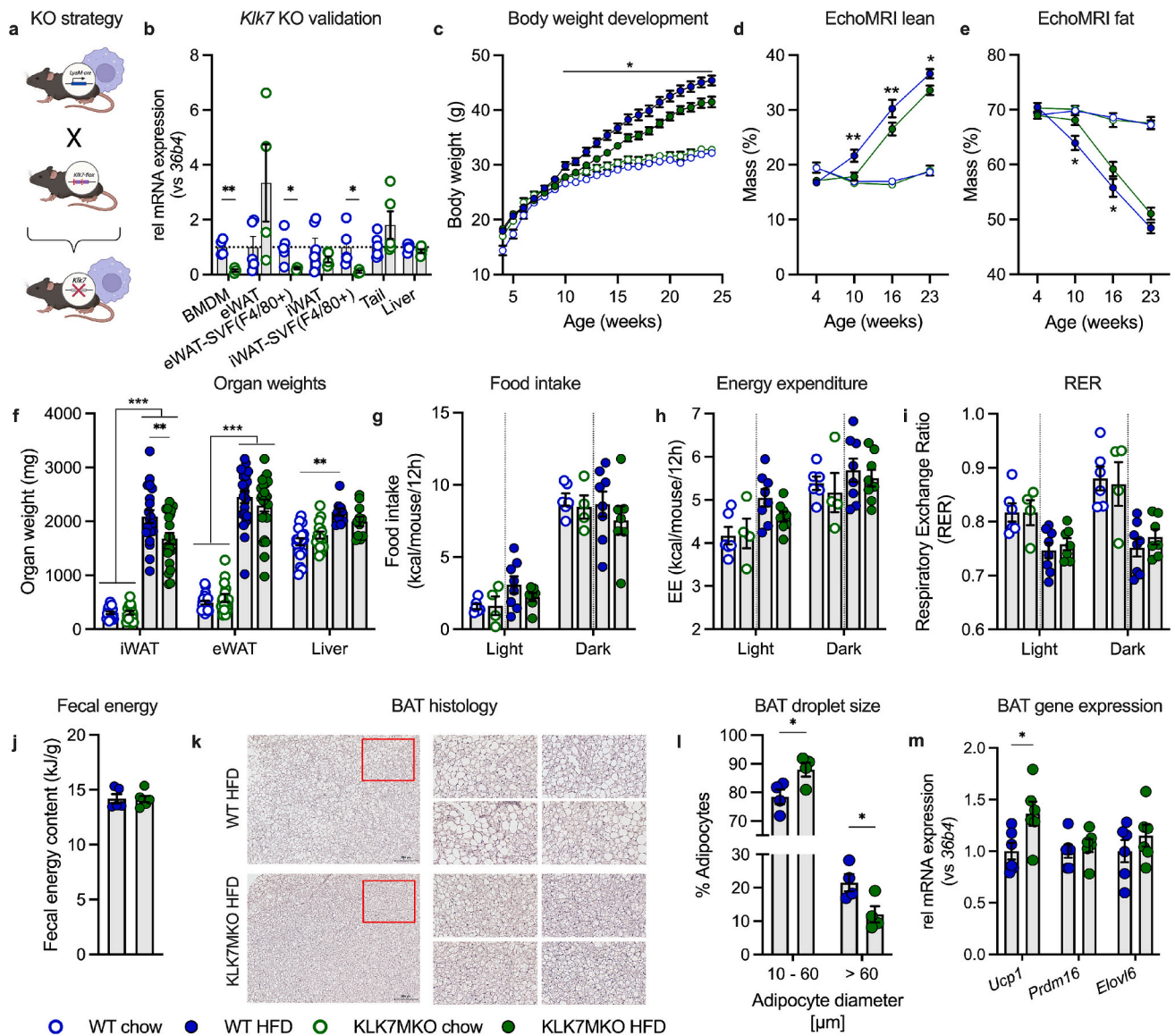


Fig. 2. *Kik7* ablation in macrophages limits high fat diet-induced obesity. a) Schematic representation of the generation of macrophage specific *Kik7* knockout mice (KLK7MKO). Mice expressing Cre-recombinase under control of the lysozyme 2 promoter (*LysM-Cre*) were crossed with C57BL6/NTac mice with conditional (floxed) *Kik7* alleles (*Kik7-flox*) to specifically delete *Kik7* in the myeloid cell lineage. b) RT-PCR analysis of *Kik7* expression in whole cell lysates from tail, liver, eWAT or iWAT; and macrophages from different anatomic sources (ATMs and BMDM) from chow-fed WT and *Kik7* knockout (KLK7MKO) mice ($n = 5-6$) reveals the specificity and efficiency of the KLK7MKO model (a). mRNA levels are relative to chow-fed WT mice for each tissue. c) Body weight development over time in KLK7MKO mice and WT littermates fed on a chow or high fat diet (HFD) for 20 weeks starting at the age of 5 weeks ($n = 12-18$ per genotype) unravels genotypic differences in HFD-fed mice. d-e) Percentage of lean (d) and fat mass (e) as determined by EchoMRI at 4, 10, 16 and 23 weeks of age from chow-fed and HFD-fed KLK7MKO mice and WT littermates ($n = 10-12$ per genotype) unravels genotypic differences in HFD-fed mice. (f) Absolute organ masses (milligrams of tissue) from iWAT, eWAT and liver from chow-fed and HFD-fed KLK7MKO mice and WT littermates ($n = 8-15$ per genotype and diet) unravel genotypic differences in iWAT from HFD-fed mice. g-i) Food intake (g), energy expenditure (h) and respiratory exchange ratio (i) from chow-fed and HFD-fed KLK7MKO and WT mice recorded every 5 min over a period of 72 h ($n = 4-8$ per genotype and diet) by indirect calorimetry (with metabolic chambers) at an age of 24 weeks and after two days of acclimatization. Data is confined in light or dark phases corresponding to the 12 h light/dark cycle. Energy expenditure was analyzed using ANCOVA with body weight as a covariate. (j) Fecal energy content from HFD-fed KLK7MKO mice and WT littermates ($n = 5$ per genotype) measured via Bomb Calorimetry. (k-l) Representative H&E staining of BAT (k) from HFD-fed KLK7MKO mice and WT littermates ($20\times$ magnification, scale = $200\mu\text{m}$) and measurements of adipocyte diameters (l) ($n = 5/4$ per genotype) reveal significantly higher numbers of enlarged droplets in BAT of WT littermates. m) RT-PCR analysis of thermogenic genes (*Ucp1*, *Prdm16* and *Elovl6*) in BAT shows increased expression of *Ucp1* in BAT of HFD-fed KLK7MKO compared to WT littermates ($n = 6$ per genotype). mRNA levels are relative to WT littermates. Genotypes are illustrated in blue (WT) and green (KLK7MKO) with diets indicated by outlined (chow) or filled (HFD) symbols. Significance ($p < 0.05$) was determined by multiple uncorrected unpaired two-tailed *t*-test (b, l-m), two-way ANOVA with Sidak's (c-e) or Tukey's post-tests (f-i) and unpaired two-tailed *t*-test (j). (For interpretation of the references to colour in this figure legend, the reader is referred to the web version of this article.)

KLK7MKO and WT controls (Fig. 4c). Histological analyses further revealed a significantly higher percentage of smaller adipocytes in eWAT of KLK7MKO compared to WT mice (Fig. 4d-e), also in iWAT of HFD-fed KLK7MKO mice (Fig. 4f). Consistently, immune cell infiltration was significantly lower compared to WT mice (Fig. 4d,g-h), with a shift

in macrophage polarization from M1 towards M2 macrophages (Fig. 4i), resulting in a lower M1/M2 ratio in eWAT of HFD-fed KLK7MKO mice (Fig. 4j). As for the ITT, mice were selected for similar body weights. In line with this hypothesis, we observed lower expression of pro-inflammatory *Tnfa* ($p < 0.05$) and *Il1b* (tendency) and significantly

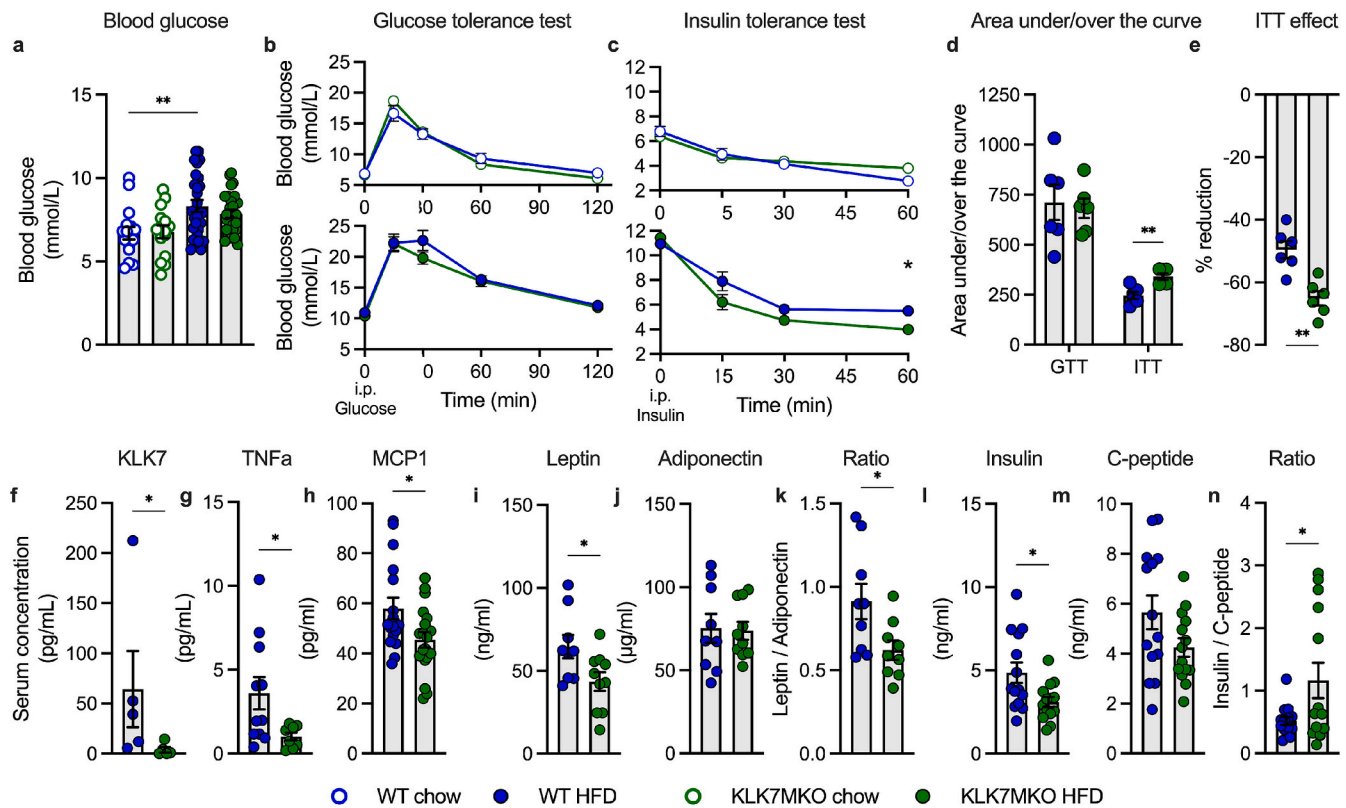


Fig. 3. *Klk7* ablation in macrophages ameliorates metabolic consequences of diet-induced obesity. a) Fasted glucose levels in KLK7MKO mice and WT littermates under chow and HFD conditions ($n = 15\text{--}28$ per genotype) measured at the age of 22 weeks. b-e) Intraperitoneal glucose (b) and insulin (c) tolerance tests (GTT at 22 weeks and ITT at 24 weeks of age), areas under/over the curve (d) and ITT effect (5 decrease of blood glucose levels after 60 min (e)) reveals higher insulin sensitivity in HFD-fed KLK7MKO mice compared to WT littermates ($n = 6\text{--}8$ per genotype). f-n) ELISA measurements in serum of KLK7MKO mice and WT littermates after 20 weeks on a HFD: (f) KLK7 levels ($n = 5$ per genotype), (g) TNF α , and (h) MCP1 ($n = 8\text{--}19$ per genotype); (i) leptin, (j) adiponectin and (k) resulting leptin/adiponectin ratio ($n = 9\text{--}10$ per genotype); (l) insulin, (m) C-peptide and (n) resulting insulin/c-peptide ratio ($n = 13\text{--}14$ per genotype) establish an overall improved metabolic phenotype of HFD-fed KLK7MKO mice compared to WT littermates. Genotypes are illustrated in blue (WT) and green (KLK7MKO), diets by outlined (chow) or filled (HFD) symbols. Significance ($p < 0.05$) was determined by one-way ANOVA and Tukey's post-test (a), two-way ANOVA with Sidak's post-test (b-c) or unpaired two-tailed t-tests (d-n). (For interpretation of the references to colour in this figure legend, the reader is referred to the web version of this article.)

higher expression of the anti-inflammatory marker *Retnla* in the eWAT-ATM (Fig. 4k) and iWAT-ATM fractions (Fig. 4l), as well as whole AT lysates from eWAT and iWAT of HFD-fed KLK7MKO mice (Fig. 4m). Because we did not detect any related effects of KLK7 depletion in the liver (Fig. 4m), we conclude that the resistance to obesity-induced inflammation in HFD-fed KLK7MKO mice is specific to AT.

To further demonstrate direct effects of KLK7 on macrophage phenotypes, we treated ATM from chow-fed WT mice with recombinant KLK7 for 24 h ex vivo. The presence of KLK7 significantly induced expression of *Mcp1* in eWAT-, but not iWAT-derived ATM (Fig. 4n). Also, KLK7 significantly reduced expression of anti-inflammatory *Retnla* in M1-polarized eWAT ATM from chow-fed WT mice (Fig. 4o).

These findings establish the pro-inflammatory role of KLK7 in stimulating or fostering immune cell infiltration of AT in obesity.

3.4. Inhibition of *Klk7* in macrophages alters migration and metabolism in the context of obesity

We next asked whether the lower immune cell infiltration in AT of HFD-fed KLK7MKO mice resulted from migration deficiencies. To answer this question, we conducted migration assays using CM from eWAT of either HFD-fed KLK7MKO (CM-KO) or WT mice (CM-WT) (Fig. 5a). In line with lower MCP1 levels observed in serum (Fig. 3f) and eWAT (Fig. 4b-c), concentrations of MCP1 were significantly lower in CM-KO compared to CM-WT (Fig. 5b) and less effective at inducing migration (Fig. 5c). Furthermore, the migratory potential of BMDM from KLK7MKO mice stimulated with CM-WT was significantly reduced

(Fig. 5c). When we analyzed migration of BMDM isolated from HFD-fed mice using only CM-WT as a chemoattractant, again the migratory potential of BMDM from KLK7MKO mice was lower than that of BMDM derived from WT mice (Fig. 5d). As assessed by electric cell substrate impedance sensing (ECIS), BMDM from KLK7MKO mice adhered more strongly to the tissue plate (Fig. 5e), but this effect was not due to higher cell proliferation (SF2a).

Energy for cytoskeletal remodeling and cell migration is derived from mitochondrial metabolism. We analyzed the metabolic activity of BMDM populations using a Seahorse extracellular flux analyzer. Oxygen consumption rates (OCR) and extracellular acidification (ECAR) were significantly higher in BMDM derived from HFD-fed WT mice relative to BMDM from chow-fed mice (Fig. 5f-h), indicating higher oxidative phosphorylation and glycolysis. This elevated metabolic phenotype was absent in BMDM from HFD-fed KLK7MKO, that instead resembled BMDM derived from chow-fed mice irrespective of genotype (Fig. 5i). Consequently, basal and maximal respiration, spare respiratory capacity, and ATP production in BMDM from HFD-fed KLK7MKO mice was comparable to that observed in chow-fed mice (Fig. 5g). In line with the less energetic phenotype, BMDM from HFD-fed KLK7MKO mice contained lower ROS levels compared to BMDM derived from HFD-fed WT mice (Fig. 5j). BMDM from KLK7MKO mice showed no differences in mitochondrial content (SF2b) or mitochondrial gene expression (SF2c) compared to WT littermates under both chow and HFD conditions. Together, these data show that immune cell migration is negatively impacted by lower expression of KLK7, likely due to higher cell adhesion in general and a lower metabolic activation in obesity.

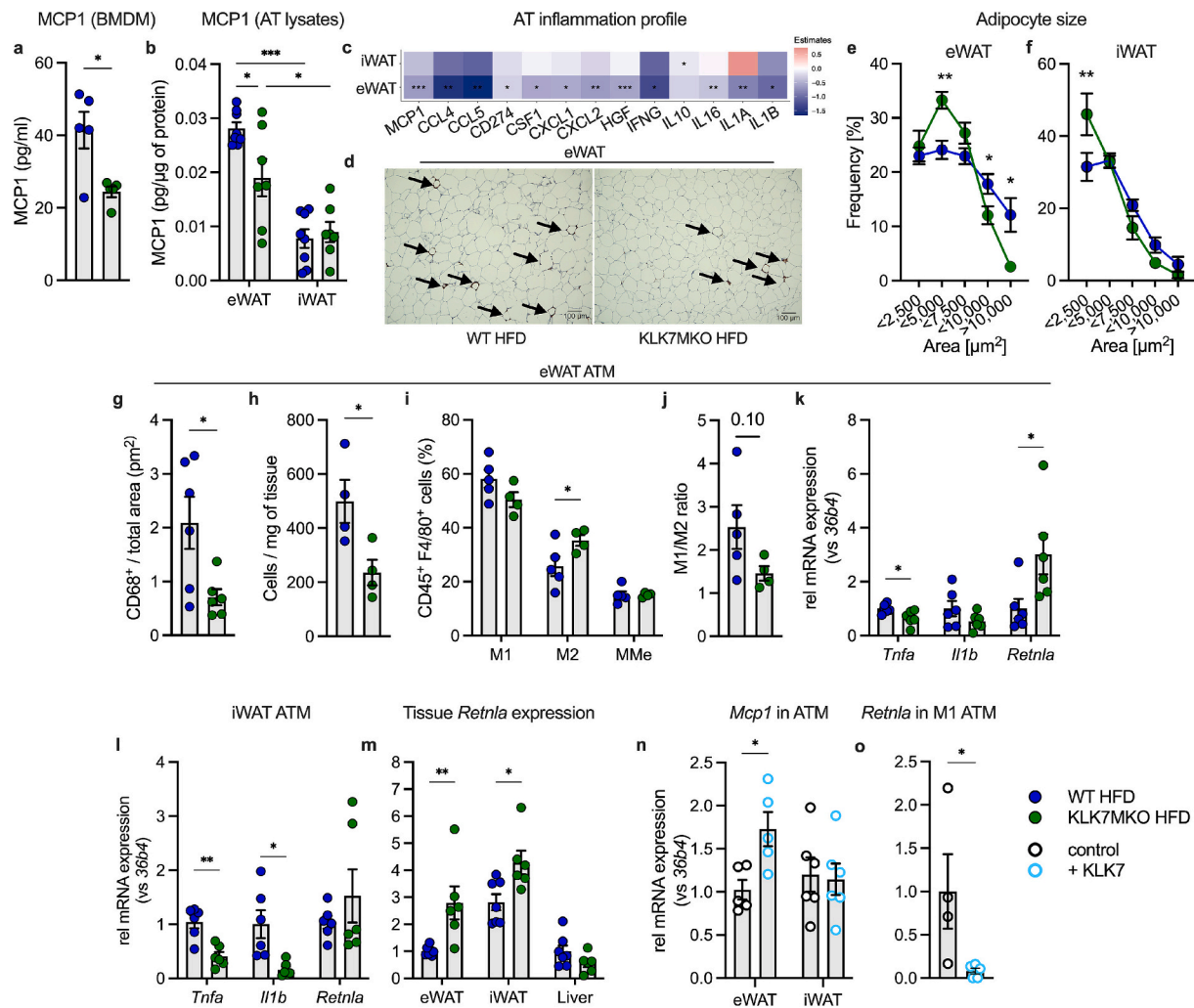


Fig. 4. *Klk7* ablation in macrophages alters adipose tissue macrophage infiltration and polarization. a) ELISA measurement reveals lower MCP1 released from naïve M0 BMDM from HFD-fed KLK7MKO mice when compared to WT littermates ($n = 5$ per genotype). b) ELISA measurements in epididymal (eWAT) and inguinal (iWAT) adipose tissue lysates reveal lower MCP1 levels specifically in the eWAT from HFD-fed KLK7MKO mice when compared to WT littermates ($n = 7-8$ per genotype). c) Normalized pro-inflammatory cytokines abundance significantly differentially expressed across adipose tissue lysates (eWAT and iWAT) and measured via the Olink Target 48 panel unravel a fat-pad specific reduction in HFD-fed KLK7MKO mice when compared WT littermates ($n = 7-8$ per genotype). d) Representative CD68 staining reveals a reduction in the presence of infiltrated macrophages in the eWAT from HFD-fed KLK7MKO mice when compared to WT littermates ($20\times$ magnification, scale = $100\mu\text{m}$). e-f) Analysis of the adipocyte size (expressed as area) distribution determined from H&E stained slides reveals a higher number of smaller and a lower number of bigger adipocytes in eWAT and iWAT from HFD-fed KLK7MKO mice when compared to WT littermates ($n = 5$ per genotype). g) Corresponding quantification from (d) reveals a reduction in the CD68⁺ area of eWAT stained slides from HFD-fed KLK7MKO mice when compared to WT littermates ($n = 6$ per genotype). h) Quantification of ATM (enriched in F4/80) isolated from eWAT reveals a reduction in HFD-fed KLK7MKO mice when compared to WT littermates ($n = 4-5$ per genotype). i-j) Quantification of fluorescence activated cell sorting of eWAT-ATM with different polarization states (M1, M2 and MMe) determined through specific cell-surface markers (CD11c, CD206 and LAMP-1/CD36 respectively) reveals a higher percentage of M2 polarized ATM in the eWAT from HFD-fed KLK7MKO mice when compared to WT littermates ($n = 4$ per genotype) (i); and corresponding M1/M2 ratio (j). k-l) RT-PCR analysis of pro- (*Tnfa* and *Il1b*) and anti- (*Retnla*) inflammatory marker genes in eWAT (k) and iWAT ATM (l) reveals lower levels of inflammation in HFD-fed KLK7MKO mice when compared to WT littermates ($n = 6$ per genotype). mRNA levels are relative to WT littermates. m) RT-PCR analysis of *Retnla* expression in liver, eWAT and iWAT tissue from HFD-fed KLK7MKO mice and WT littermates ($n = 5-6$ per genotype). mRNA levels are relative to WT littermates (WAT to eWAT). n) RT-PCR analysis in ATM (from eWAT and iWAT) from chow-fed WT littermates treated with recombinant KLK7 over 24 h ($n = 5-6$ per group) reveals a fat-pad specific induction of *Mcp1* in eWAT-ATM. mRNA levels are relative to eWAT controls. o) RT-PCR analysis in eWAT-ATM from chow-fed WT mice polarized to M1 while treated with recombinant KLK7 over 24 h ($n = 4-5$ per group) reveals a lower *Retnla* expression in the treated group. Genotypes and treatments are illustrated in blue (WT) and green (KLK7MKO), black (control) and turquoise (KLK7). Significance ($p < 0.05$) was determined by unpaired two-tailed *t*-test (a,g,h,j,o), multiple unpaired uncorrected two-tailed *t*-tests (e,f,k-m), two-way ANOVA with Tukey's (b), or uncorrected Fischer's LSD (i). (For interpretation of the references to colour in this figure legend, the reader is referred to the web version of this article.)

3.5. *KLK7* expression in human visceral adipose tissue is linked to inflammation and adipose immune cell infiltration in obesity

To investigate the clinical relevance of our findings, we analyzed *KLK7* levels in human serum and WAT depots. In human scRNA-seq datasets [55], we found significant levels of *KLK7* in the visceral AT, but not subcutaneous (SC) AT (Fig. 6a). *KLK7* was strongly expressed in

visceral AT mesothelial cells, and was also detectable in macrophages, T-cells, adipocytes and adipose stem and progenitor cells (ASPC) (Fig. 6a). PBMC derived M0 macrophages from patients with obesity also secreted/contained significantly higher levels of *KLK7* (Fig. 6b). We further analyzed *KLK7* expression in 1143 human VIS and SC AT samples from the cross-sectional cohort of the Leipzig Obesity BioBank (LOBB). We found that *KLK7* expression was significantly higher in VIS

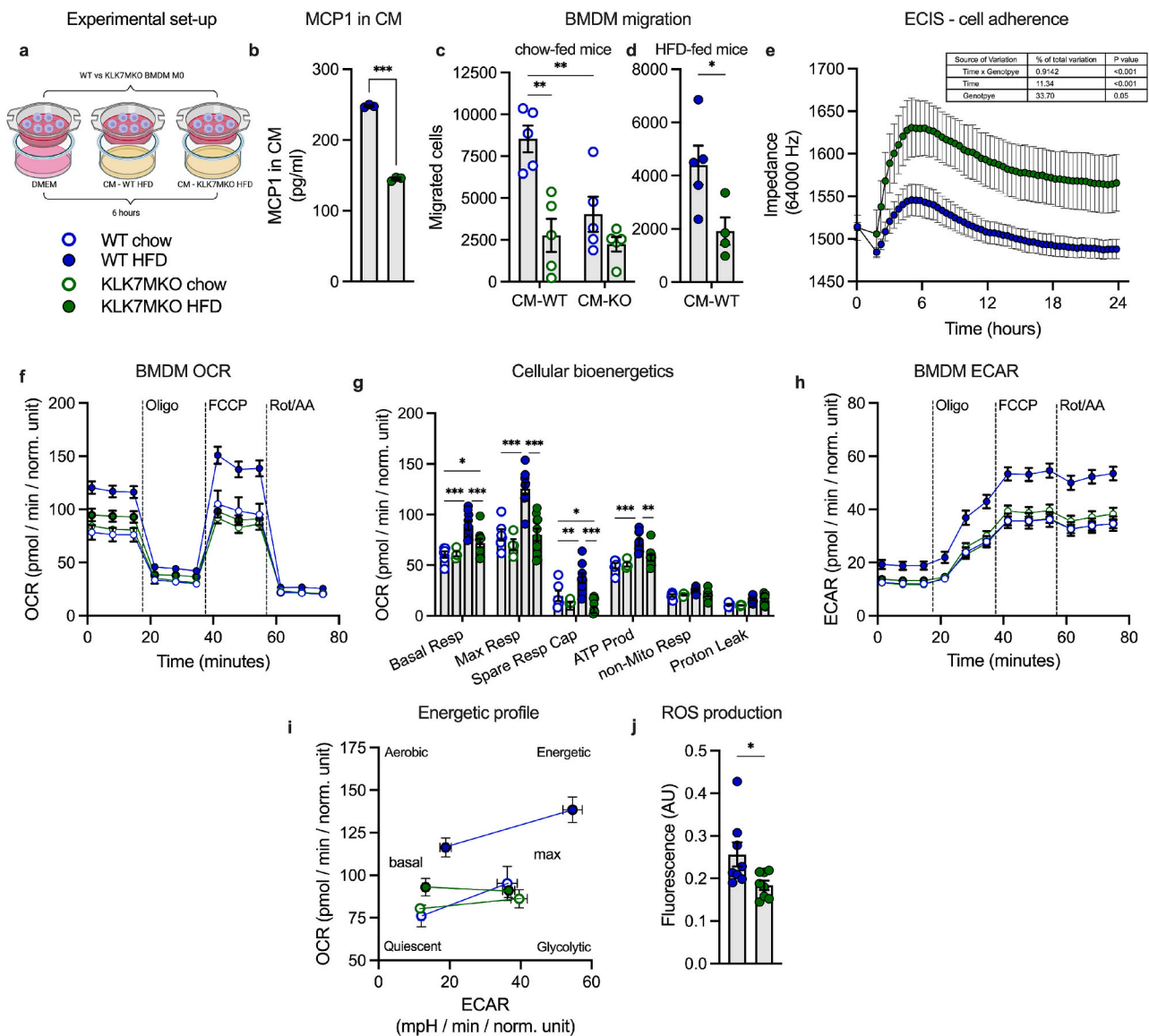


Fig. 5. *Klk7* ablation in macrophages affects migratory capacity and alters immune cell metabolism in obesity. a) Experimental set-up using trans-well inserts to assess the effect of conditioned media (CM) during 6 h, obtained from eWAT explants of HFD-fed *KLK7MKO* mice and WT littermates, on BMDM migration from chow and HFD-fed *KLK7MKO* mice and WT littermates. b) ELISA measurement reveals lower levels of MCP1 in conditioned media from eWAT explants of *KLK7MKO* mice when compared to WT littermates (CM-WT or CM-KO; $n = 3$ technical replicates from pooled samples). c) Quantification of migration as in (a) reveals a lower migration capacity of BMDM from chow-fed *KLK7MKO* mice when compared to WT littermates ($n = 5$ per genotype and diet); and a lower chemo-attractant effect of HFD-fed *KLK7MKO* derived-CM when compared to HFD-fed WT derived-CM. d) Quantification of BMDM migration as in (a), but with BMDM from HFD-fed mice and using WT-CM reveals a lower migration capacity of BMDM from *KLK7MKO* mice when compared to WT littermates ($n = 4-5$ per genotype). e) Cell impedance to continuously measure cell adhesion over 24 h (using a constant current of 64,000 Hz) in BMDM from HFD-fed *KLK7MKO* mice and WT littermates ($n = 5$ per genotype). f-h) Time-resolved analysis of the Oxygen Consumption Rate (OCR) (f), quantification of corresponding cellular bioenergetics (basal and maximal respiration, spare respiratory capacity, ATP production, non-mitochondrial respiration, and proton leak, g) and analysis of the time-resolved Extracellular Acidification Rate (ECAR) (h) in BMDM from chow-fed and HFD-fed *KLK7MKO* mice and WT littermates ($n = 3-5$ chow-fed and $n = 8-9$ HFD-fed animals per genotype) measured via the Mito Stress test using a Seahorse extracellular flux analyzer unravels genotypic differences in BMDM from HFD-fed mice. i) Energetic profile map derived from (f) and (g). j) ROS production in BMDM from HFD-fed *KLK7MKO* mice and WT littermates ($n = 8$ per genotype) reveals genotypic differences. Genotypes are illustrated in blue (WT) and green (*KLK7MKO*), diets by outlined (chow) or filled (HFD) symbols. Significance ($p < 0.05$) was determined by unpaired two-tailed t-test (b,d,j) and two-way ANOVA with Tukey's post-test (c) or uncorrected Fischer's LSD (e,g). (For interpretation of the references to colour in this figure legend, the reader is referred to the web version of this article.)

relative to SC AT in patients with obesity (Fig. 6c; adj. $p < 0.001$), and independent of diabetes status (SF3a, no T2D: adj. $p < 0.001$, IFG/IGT: adj. $p < 0.001$, T2D: adj. $p < 0.001$) and gender (SF3b; men: adj. $p < 0.001$; women: adj. $p < 0.001$). In VIS AT, there was a trend for higher *KLK7* expression in patients with obesity ($p = 0.06$), and for lower *KLK7* expression in patients with T2D ($p = 0.04$). Age- and sex-adjusted *KLK7* expression was significantly correlated with body fat in VIS AT (Fig. 6d, $\rho = 0.09$, $p = 0.0018$, $n = 1112$).

We then identified genes significantly correlated with *KLK7* expression in VIS and SC AT and performed gene set enrichment analyses (GSEA) using the KEGG pathway database (Fig. 6e; Supplementary table 2 for VIS AT, and Supplementary table 3 for SC AT). In VIS AT, *KLK7* expression correlated positively with genes enriched in pathways related to cell migration and cell adhesion molecules (NES = 1.9, adj. $p = 0.0015$), chemokine signaling (NES = 2.3, adj. $p = 0.0015$), focal adhesion (NES = 2.6, adj. $p = 0.0015$) and regulation of actin

human AT KLK7 expression

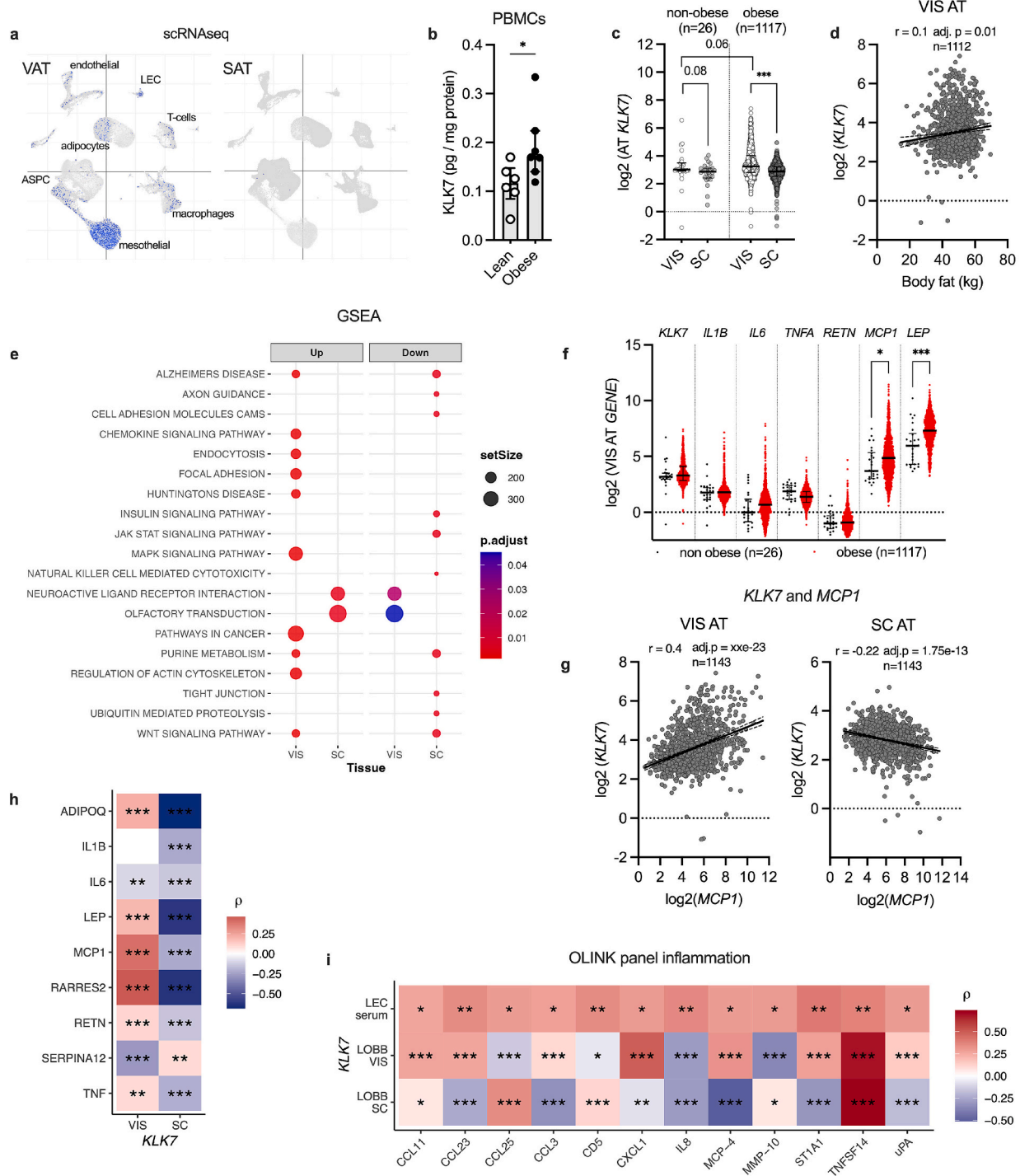


Fig. 6. KLK7 expression in human AT and serum is linked to inflammation and immune cell migration. a) KLK7 expression in human VIS and SC AT at the single cell level. Data was from [55]. b) ELISA measurement reveals higher released levels of KLK7 from PBMCs isolated from participants with obesity (n = 7) and cultured over 10 days when compared to PBMCs isolated from participants without obesity (n = 6) from the Tarragona cohort. c) RNA sequencing analysis of KLK7 expression in VIS and SC AT of participants with (n = 1117) or without obesity (n = 26) from the Leipzig Obesity BioBank (LOBB) cohort reveals AT depot specific KLK7 induction in participants with obesity. d) Spearman correlation analysis of KLK7 and body fat in VIS AT (adjusted for age and sex) reveals a positive correlation between the RNA levels of KLK7 and the body fat of the participants from the LOBB cohort (n = 1112). e) Gene set enrichment analysis (GSEA, using KEGG pathways) of genes co-expressed with KLK7 in VIS and SC AT from the LOBB cohort. The top 10 up and down enriched pathways sorted by adj. p and set size are shown. f) Comparison of gene expression of KLK7, inflammatory cytokines (IL1B, IL6, TNFA, RETN and MCP1) and the adipokine LEP in VIS AT in non-obese and obese patients. g) Correlations of KLK7 and MCP1 expression in VIS (left) and SC (right) AT from the LOBB cohort (adjusted for age and sex) reveal depot-specific differences. h) Correlation analysis of KLK7 expression with Spearman's correlation in VIS and SC AT from the LOBB cohort with inflammatory cytokines and adipokines (corrected for multiple testing). i) Correlations shared between KLK7 and inflammatory biomarkers in serum from the Leipzig Endocrinology cohort and AT depots from the LOBB cohort reveal markers strongly associated with KLK7. Significance (p < 0.05) was determined by unpaired two-tailed t-test (b) or one-way ANOVA (c).

cytoskeleton (NES = 2.4, adj. $p = 0.0014$). Furthermore, genes related to WNT signaling (NES = 2.5, adj. $p = 0.0014$), MAPK signaling (NES = 2.3, adj. $p = 0.0015$) and purine metabolism (NES = 2.4, adj. $p = 0.0015$) were overrepresented among positively correlated genes. Conversely, genes related to olfactory transduction (NES = -3.5, adj. $p = 0.045$) and neuroactive ligand receptor interactions (NES = -1.9, adj. $p = 0.029$) were negatively correlated with *KLK7* expression in VIS AT. In SC AT, *KLK7* was associated with higher expression of genes related to neuroactive ligand receptor interactions (NES = 1.8, adj. $p = 0.00066$) and olfactory transduction (NES = -2.5, adj. $p = 0.0039$), while negatively correlated genes were related to insulin signaling (NES = -2.8, adj. $p = 0.004$), WNT signaling (NES = -2.3, adj. $p = 0.0039$), and purine metabolism (NES = -2.4, adj. $p = 0.0039$).

In relation to classic adipokines and inflammatory cytokines (such as *IL1B*, *IL6*, *RETN*, *MCP1* and *LEP*), *KLK7* was robustly expressed in human VIS AT (Fig. 6f). Notably, of these candidates only *MCP1* and *LEP* were significantly higher expressed in patients with obesity (Fig. 6f). Given on our findings in the *KLK7*MKO mouse model, that *KLK7* depletion in the myeloid compartment reduces inflammation, we next investigated a possible link between AT *KLK7* gene expression and genes related to AT function and inflammation (Supplementary table 4). In VIS AT ($n = 1143$), we indeed detected a strong correlation between *KLK7* and *MCP1* expression ($\rho = 0.4$, adj. $p < e^{-23}$; Fig. 6g-h), independent of age and sex. *KLK7* was also positively correlated with *ADIPOQ* ($\rho = 0.21$, $p = 8.5e^{-13}$), *LEP* ($\rho = 0.19$, adj. $p = 1.2e^{-10}$), *RARRES2* ($\rho = 0.46$, adj. $p < e^{-23}$), *RETN* ($\rho = 0.1$, adj. $p = 0.00065$) and *TNF α* ($\rho = 0.1$, adj. $p = 0.0023$), and negatively correlated with *IL6* ($\rho = -0.1$, adj. $p = 0.0013$) and a specific vaspin inhibitor (*SERPINA12*; $\rho = -0.28$, adj. $p = 6.5e^{-21}$) (Fig. 6h, Supplementary table 4). In SC AT, *KLK7* was also correlated with *MCP1* ($\rho = -0.21$, adj. $p = 1.7 \times 10^{-13}$), *TNFA* ($\rho = -0.21$, adj. $p = 9.8e^{-13}$) and vaspin (*SERPINA12*, $\rho = 0.1$, adj. $p = 0.0014$), but in the opposite direction relative to VIS AT (Fig. 6g-h, Supplementary table 4). Furthermore, *KLK7* was negatively correlated with *ADIPOQ* ($\rho = -0.68$, adj. $p < e^{-23}$), *LEP* ($\rho = -0.62$, adj. $p < e^{-23}$), *IL1B* ($\rho = -0.23$, adj. $p = 2.6e^{-14}$), *IL6* ($\rho = -0.13$, adj. $p = 4.8e^{-6}$), *RARRES2* ($\rho = -0.63$, adj. $p < e^{-23}$), and *RETN* ($\rho = -0.15$, adj. $p = 3.9e^{-7}$) (Fig. 6h, Supplementary table 4).

To investigate the interrelation of circulating *KLK7* with (systemic) inflammation, we measured *KLK7* levels in the serum of a well characterized second cohort with available targeted OLINK protein expression data. This cohort of 60 individuals comprises patients with or without T2D and with a wide BMI range (25 % percentile = 26.7, median = 28.7, 75 % percentile = 31.9). There were no differences in circulating *KLK7* levels related to sex, BMI, age or diabetes status (SF3c-f), and there were no significant correlations of circulating *KLK7* with other clinical parameters of obesity and metabolic health (Supplementary table 5). As observed in VIS AT gene expression, serum *KLK7* levels were positively correlated with circulating chemerin ($\rho = 0.36$, adj. $p = 0.00031$, SF3g). When we investigated correlations between *KLK7* and a broad panel of inflammatory serum biomarkers included in the OLINK Target 96 inflammation panel ($n = 82$ included in this analysis), we identified 14 markers (nominal $p < 0.05$) (Supplementary table 6, SF3h), with *CCL23*, *CD5*, *IL8*, *ST1A1* and *TNFSF14* showing the strongest correlations. We then performed a complementary panel-wide association analysis for *KLK7* VIS and SC AT gene expression in the LOBB cohort. We identified 79 inflammatory genes that significantly correlated with *KLK7* expression, 64 of which are expressed in both VIS and SC AT, and 45 of which have a differential expression profile in the AT depots (Supplementary table 6). 12 markers were significantly correlated with *KLK7* in serum of the Leipzig Endocrinology cohort and with *KLK7* gene expression in both AT depots of the LOBB cohort (Fig. 6i, SF3h; Supplementary table 6). The strongest and uniformly positive correlation was with *TNFSF14* (Fig. 6i), an established driver of AT inflammation and metabolic disease in obesity [56,57]. Consistent correlations were mostly observed between serum and VIS AT, while only two markers were correlated uniformly in serum and SC AT (Fig. 6i; Supplementary table 6).

Together, these results support the hypothesis that elevated *KLK7* expression levels in AT are functionally related to inflammation in VIS AT and may be linked to immune cell infiltration of adipose tissue in human obesity. At the serum level, we found significant associations with established inflammatory markers mostly in line with VIS AT gene expression. And although serum *KLK7* was not directly linked to obesity or T2D, we observed the strongest and most uniform correlations between key regulators of immune cell activation and adipose tissue inflammation.

4. Discussion

Immune cell infiltration and inflammation, hallmarks of adipose tissue dysfunction, are drivers of metabolic abnormalities in animal models of obesity and in human obesity. In this study, we demonstrate that myeloid-specific deletion of *Klk7* in HFD mice is associated with lower levels of inflammatory cytokines in epididymal AT as well as in serum, and with lower immune cell infiltration with proportionally more anti-inflammatory M2 macrophages in AT. At the end of our study, these improvements had a significant effect on insulin sensitivity, yet a more limited impact on fasting glucose levels and glucose tolerance. This is consistent with the findings in the AT-specific (using *Fabp4-Cre*) *KLK7* knockout mice [41] and may require prolonged HFD-feeding to have more pronounced effects on metabolic parameters. Furthermore, it may reflect that *KLK7* expression in pancreatic islets, known to affect levels of secreted insulin [22], or in mesothelial cells of the visceral AT (Fig. 6a), a cell population strongly linked to AT inflammation [58,59], is not altered in the myeloid-specific *KLK7*MKO. Importantly, amelioration of metabolic inflammation in epididymal AT in the macrophage *KLK7*MKO mice occurred despite predominant loss of iWAT and thus a shift towards visceral obesity, distinct from the adipocyte-specific *Klk7* knockout in which subcutaneous obesity was more pronounced [31]. Higher adaptive thermogenesis and improved BAT function, likely preserved by reduced inflammation, may contribute to the lower body weight gain in *KLK7*KO models on HFD. However, as indicated by the ECHO-MRI fat mass data at 6 and 10 weeks, differences in energy expenditure may have been most pronounced early on the HFD diet and may decline over time due to adaptation.

Supporting a functional role of *KLK7* in shifting macrophage polarization, our data show that *Klk7*-deficient macrophages express and release lower levels of the inflammatory cytokines *Mcp1*, *Trfa* and *Il1b* and higher levels of the anti-inflammatory M2 macrophage marker *Retnla* [60]. In obesity, *Retnla*-expressing monocytes and macrophages are gradually replaced by other ATM subpopulations, including lipid-catabolizing macrophages that form crown-like structures surrounding hypertrophic adipocytes [61]. Consistent with a predominantly anti-inflammatory M2-like phenotype, the cellular metabolism of *Klk7*-deficient macrophages from HFD-fed mice retained a less glycolytic profile. Mechanistically, *KLK7* activity may drive inflammatory polarization by directly activating established cytokine and adipokine mediators of inflammation, such as *IL1b* [62], chemerin [63], and midkine [64].

Obesity-related local and systemic inflammation is exacerbated by higher infiltration of circulating monocytes into adipose tissue [65] and their subsequent differentiation into proinflammatory macrophages. Our data show that *Klk7*-deficient BMDM become more adhesive, limiting their ability to migrate towards a chemoattractant gradient and infiltrate AT. Higher expression of cadherin-related proteins was previously observed in the WAT of HFD-fed *KLK7* KO mice [30] suggesting that *KLK7* may contribute to regulate shedding of cell surface ECM adhesion molecule. *KLK7*-mediated shedding of E-cadherin and fibronectin has also been proposed to promote cancer cell migration and invasion [66,67], with high levels of *KLK7* expression being associated with poor prognosis across several solid tumor indications [68–70]. In line, overexpression of *KLK7* in epidermal cells induced inflammatory skin thickening due to infiltration of predominantly macrophages [71].

Furthermore, higher E-cadherin expression is a hallmark of alternatively activated M2 macrophages, enhancing cell-cell adhesion, and when accumulated in the extracellular matrix, promoting fibroblast and endothelial cell spreading [72]. Similarly, known KLK7 substrates such as the ECM glycoproteins fibronectin and tenascin-C [64] are expressed in human macrophages, mediate cell-cell adhesion and migration [73–75], and are associated with AT inflammation in human obesity [76,77].

Other proteases identified to drive AT inflammation in obesity, such as neutrophil elastase or fibroblast activation protein α (FAP), promote immune cell infiltration but without affecting macrophage polarization [12,78]. Also, FAP knock-out in immune cells significantly improved AT inflammation and insulin resistance in HFD-fed mice, but also limited body weight gain and reduced visceral obesity, and thus complicate delineating contributions from FAP deficiency from those of less pronounced obesity [78]. Similarly, this holds true for whole-body elastase knock-out mice [12]. Inhibition of KLK7 may thus be particularly beneficial, as it addresses both inflammatory polarization of local immune cells and the infiltration of additional immune cells in visceral obesity.

KLK7 inhibitors are being actively developed to address inflammatory skin diseases, cancers, and other conditions where KLK7 dysregulation drives pathology, with potential applications in respiratory diseases and wound healing due to its role in inflammation and tissue remodeling. Inhibitors, ranging from small molecules to antibodies, are currently in clinical trials, particularly for skin disorders, pancreatitis, and asthma. Intriguingly, the natural product tutuilamide A, a 3-amino-6-hydroxy-2-piperidone cyclodepsipeptide derived from marine cyanobacteria, has been shown to exhibit excellent selectivity towards human neutrophil elastase and KLK7, also discriminating KLK7 from other KLK homologs with excellent selectivity [79]. Given the beneficial effects of neutrophil elastase and KLK7 inhibition or knockout in diet-induced obese mice, compounds like this would be extremely interesting to study in the context of obesity. However, validating KLK7 as a pharmaceutical target for the treatment of obesity-related metabolic disorders in mouse models poses several challenges. Foremost, species differences in the specificity pocket of the protease active site (human: Ala190, mouse: Thr190) render most inhibitors inefficient when targeting mouse KLK7 and would therefore require humanized KLK7 mouse models. Alternatively, inhibitors must be designed to overcome these species differences, and initial efforts have already been reported [80].

Human adipose tissue expression data further supports the link between KLK7 expression and inflammation, highlighting its potential as a therapeutic target in human obesity. Analyzing WAT KLK7 expression and serum KLK7 levels in two cohorts, we found that KLK7 expression is significantly higher in VIS AT relative to SC AT, independent of diabetes or obesity status. This expression difference is consistent with the visceral AT-specific effects we observed in KLK7MKO mice, but also reflects the visceral AT-specific presence of mesothelial cells, which in addition to VAT macrophages express high levels of KLK7 (Fig. 6a) [55]. KLK7 expression correlated with pro-inflammatory cytokines in AT and consistent with our in vivo findings, KLK7 expression in VIS was significantly associated with *MCP1* and *TNFA*. In more comprehensive analyses (including gene expression of proteins measured by the OLINK inflammation panel), we found significant correlations between KLK7 and a multitude of inflammatory mediators in both AT depots, the majority of which were differentially regulated in VIS and SC AT, and only 8 with the same expression profile in both AT depots (Supplementary table 6). The most strongly associated genes in VIS AT were established mediators of obesity-related inflammation, such as *CXCL6*, *CD40*, *IL-18*, *TRAIL*, *bNGF* and others. The neutrophil-recruiting chemokine GCP-2/*CXCL6* [81] is a driver of early neutrophil infiltration into visceral AT in response to a HFD, initiating the pro-inflammatory cascade in obese AT [82]. IL18 expression is induced by proinflammatory cytokines such as TNFA in human adipocytes and is associated with inflammation and insulin resistance in human obesity [83,84]. Similarly, NGF is expressed

and secreted by human white adipocytes, induced by TNFA, and associated with inflammatory response in AT [85]. TNFSF14, the most strongly and uniformly associated gene (in AT and serum), is increased in obesity and T2D in humans [86,87], and promotes cytokine release from adipocytes and macrophages to drive AT inflammation and onset of hepatic insulin resistance [56,57]. Yet, despite the obvious relationship between KLK7 expression and inflammation locally (in AT) and systemically (in the circulation), clinical data further indicated no clear correlations between KLK7 expression in VIS AT and obesity, BMI, or type 2 diabetes, suggesting its role in metabolic dysfunction may be context-dependent or nuanced. Our observations however may be biased by the composition of the LOBB cohort featuring predominantly individuals with high grade obesity and only a small number of individuals with normal or overweight. Furthermore, protease biology is inherently complex, as protein levels often not reflect activity due to expression as an inactive zymogen, activation by proteases or as part of protease cascades, spatial-temporal regulation, and compartmentalization. Additionally, the expression of specific inhibitors (e.g., serpins like vaspin for KLK7) and limited substrate access create dynamic regulatory patterns that challenge straightforward correlation analysis. Yet, we found human PBMCs (cultured over 10 days and enriched in attached monocytes and macrophages) from patients with obesity released significantly higher levels of KLK7 compared to lean controls, highlighting the role of this protease in obesity and specifically in immune cells. Inhibition of KLK7 activity in pancreatic islets or from visceral AT-specific mesothelial cells may further enhance the benefits of KLK7-targeted treatment strategies for metabolic diseases.

An obvious limitation of our study is that no single or specific molecular interaction or pathway can be attributed to our findings, nor can it be inferred from the significant correlations of KLK7 with inflammatory markers. Rather, the increasing number of recently identified interferon and cytokine substrates of KLK7 [64,88] further support that, in addition to its most prominent role in keratinocyte shedding in the skin, KLK7 appears to have a profound impact on complex inflammatory cytokine networks. Along these lines, already subtle changes in protease expression or activity may have non-linear effects due to cascade amplification or regulation of multiple downstream targets.

In conclusion, our work shows that obesity induces KLK7 expression in immune cells, which promotes an inflammatory macrophage profile as well as migration and infiltration of macrophages, particularly into the visceral AT in mice, and drives AT inflammation. Our work also establishes a strong link between KLK7 and inflammation in humans and suggests that proteolytic enzymes such as KLK7 are promising pharmacological targets for the treatment of AT dysfunction in obesity.

CRediT authorship contribution statement

Alex Ribas-Latre: Writing – review & editing, Writing – original draft, Visualization, Methodology, Investigation, Formal analysis, Data curation, Conceptualization. **Anne Hoffmann:** Visualization, Formal analysis, Data curation. **Claudia Gebhardt:** Validation, Investigation, Formal analysis. **Juliane Weiner:** Writing – review & editing, Validation, Investigation, Formal analysis. **Lilli Arndt:** Investigation, Formal analysis. **Nora Raulien:** Investigation, Formal analysis. **Martin Gericke:** Writing – review & editing, Investigation, Formal analysis. **Adhdeb Ghosh:** Investigation, Formal analysis, Data curation. **Kerstin Krause:** Writing – review & editing, Investigation, Formal analysis. **Nora Klötting:** Writing – review & editing, Investigation. **Paul T. Pfluger:** Writing – review & editing, Investigation. **Bilal N. Sheikh:** Writing – review & editing, Investigation, Formal analysis. **Thomas Ebert:** Writing – review & editing, Resources, Investigation, Formal analysis. **Anke Tönjes:** Writing – review & editing, Resources, Investigation. **Michael Stumvoll:** Writing – review & editing, Resources. **Christian Wolfrum:** Writing – review & editing, Resources. **Matthias Blüher:** Writing – review & editing, Resources. **Ulf Wagner:** Writing – review & editing, Formal analysis. **Joan Vendrell:** Writing – review &

editing, Resources. **Sonia Fernández-Veledo:** Writing – review & editing, Resources. **John T. Heiker:** Writing – review & editing, Writing – original draft, Visualization, Supervision, Project administration, Methodology, Funding acquisition, Formal analysis, Conceptualization.

Financial support statement

This work was supported by the Deutsche Forschungsgemeinschaft (DFG; German Research Foundation) through CRC1052 “Obesity Mechanisms”, project number 209933838 (B1 MB, B4, NK, B9 MG, B12 KK, C7 JTH), 457240345 and 511049882 (to BNS), TRR296 (to PP), WA 2765/13-1 (to UW), as well as the Free State of Saxony and Helmholtz Munich. TE was supported by the EFSD Mentorship Programme supported by AstraZeneca and the German Diabetes Association (DDG). The German Diabetes Center is funded by the German Federal Ministry of Health (Berlin, Germany) and the Ministry of Culture and Science of the state North Rhine-Westphalia (Düsseldorf, Germany) and receives additional funding by the German Federal Ministry of Education and Research (BMBF) through the German Center for Diabetes Research (DZD e.V.). PP acknowledges support from the European Research Council (ERC CoG 101002247). SF-V acknowledges support from the Spanish Ministry of Science and Innovation MCIN/AEI/10.13039/501100011033 (PID2021-122480OB-I00) and from “La Caixa” Foundation (ID 100010434) under grant agreement LCF/PR/HR20/52400013. JV acknowledges support from the Instituto de Salud Carlos III (PI20/00338 and PI23/01133). SF-V and JV acknowledge support from the CIBER -Consorcio Centro de Investigación Biomédica en Red- (CB07708/0012), Instituto de Salud Carlos III, Ministerio de Ciencia e Innovación and from the Agency for Management of University Research Grants of the Generalitat de Catalunya (2021 SGR 01409, 2021 SGR 0089).

Declaration of competing interest

The authors declare the following financial interests/personal relationships which may be considered as potential competing interests: Matthias Blueher reports a relationship with Amgen, AstraZeneca, Bayer, Boehringer-Ingelheim, Lilly, Novo Nordisk, Novartis, and Sanofi that includes: consulting or advisory and speaking and lecture fees. Thomas Ebert reports a relationship with Bayer, Boehringer Ingelheim, Fresenius Medical Care, Lilly, Novo Nordisk, Sanofi, and Santis that includes: consulting or advisory and speaking and lecture fees. Paul Pfluger reports a relationship with Novo Nordisk that includes: speaking and lecture fees. If there are other authors, they declare that they have no known competing financial interests or personal relationships that could have appeared to influence the work reported in this paper.

Acknowledgments

We acknowledge the technical support of Core Facility Metabolomics and Proteomics (CF-MPC) at Helmholtz Munich and thank Dr. Agnese Petrera and Nicole Muth. We thank Wenfei Sun and Hua Dong for supporting human adipose tissue RNA-seq, Jenny Schuster and Lisa Gärtner from the animal facility, and Lisa Roth, Kevin Möhrlis, Inka Rapöhn, Sebastian Dommel, Sophie Rehme, Olivia Paetow, Ulrike Löbner, Miriam Krekel, Lisa Christen, Fabiana Oliveira and Elsa Maymo for excellent technical assistance or experimental advice. We further thank all patients and their families for participating in this study.

Appendix A. Supplementary data

Supplementary data to this article can be found online at <https://doi.org/10.1016/j.metabol.2025.156239>.

Data availability

All the necessary data to evaluate the conclusions in the paper are provided in the paper itself and/or the Supplementary Materials. The human RNA-seq data from the LOBB study, as well as the targeted biomarker analysis from the Leipzig Endocrinology cohort, have not been deposited in a public repository due to restrictions imposed by patient consent. However, interested individuals can request access to this data from the corresponding author.

References

- [1] Mozaffarian D. Perspective: obesity-an unexplained epidemic. *Am J Clin Nutr* 2022;115:1445–50.
- [2] Allison DB, Downey M, Atkinson RL, Billington CJ, Bray GA, Eckel RH, et al. Obesity as a disease: a white paper on evidence and arguments commissioned by the Council of the Obesity Society. *Obesity (Silver Spring)* 2008;16:1161–77.
- [3] Albaugh VL, He Y, Munzberg H, Morrison CD, Yu S, Berthoud HR. Regulation of body weight: lessons learned from bariatric surgery. *Mol Metab* 2023;68:101517.
- [4] Blüher M, Aras M, Aronne LJ, Batterham RL, Giorgino F, Ji L, et al. New insights into the treatment of obesity. *Diabetes Obes Metab* 2023;25:2058–72.
- [5] Gou Y, Schwartz MW. How should we think about the unprecedented weight loss efficacy of incretin-mimetic drugs? *J Clin Invest* 2023;133.
- [6] Sun K, Kusminski CM, Scherer PE. Adipose tissue remodeling and obesity. *J Clin Invest* 2011;121:2094–101.
- [7] Xu Q, Mariman ECM, Goossens GH, Blaak EE, Jocken JWE. Cathepsin gene expression in abdominal subcutaneous adipose tissue of obese/overweight humans. *Adipocyte* 2020;9:246–52.
- [8] Naour N, Rouault C, Fellahi S, Lavoie ME, Poitou C, Keophiphat M, et al. Cathepsins in human obesity: changes in energy balance predominantly affect cathepsin S in adipose tissue and in circulation. *J Clin Endocrinol Metab* 2010;95:1861–8.
- [9] El Mesallamy HO, Hamdy NM, Mostafa DM, Amin AI. The serine protease granzyme B as an inflammatory marker, in relation to the insulin receptor cleavage in human obesity and type 2 diabetes mellitus. *J Interf Cytokine Res* 2014;34:179–86.
- [10] Cekici L, Kopp HP, Brix J, Koder S, Ay C, Scherthaler GH, et al. Thrombin generation in morbid obesity: significant reduction after weight loss. *Diabetes* 2009;58:A452-A.
- [11] Batist G, Bothe A, Bern M, Bistrrian BR, Blackburn GL. Low anti-thrombin-iii in morbid-obesity - return to normal with weight-reduction. *Jpn-Parenter Enter* 1983;7:447–9.
- [12] Mansuy-Aubert V, Zhou QL, Xie X, Gong Z, Huang JY, Khan AR, et al. Imbalance between neutrophil elastase and its inhibitor alpha1-antitrypsin in obesity alters insulin sensitivity, inflammation, and energy expenditure. *Cell Metab* 2013;17:534–48.
- [13] Wu Y, Jiang Y, Guo JQ, Yang ZW, Carvalho A, Qian LL, et al. Visceral adipose tissue-directed human kallistatin gene therapy improves adipose tissue remodeling and metabolic health in obese mice. *Cell Signal* 2023;106.
- [14] Fruhbeck G, Gomez-Ambrosi J, Rodriguez A, Ramirez B, Valenti V, Moncada R, et al. Novel protective role of kallistatin in obesity by limiting adipose tissue low grade inflammation and oxidative stress. *Metabolism* 2018;87:123–35.
- [15] Li BY, Guo YY, Xiao G, Guo L, Tang QQ. SERPINA3C ameliorates adipose tissue inflammation through the cathepsin G/integrin/AKT pathway. *Molecular Metabolism* 2022;61.
- [16] D'Souza RF, Masson SWC, Woodhead JST, James SL, MacRae C, Hedges CP, et al. alpha1-Antitrypsin A treatment attenuates neutrophil elastase accumulation and enhances insulin sensitivity in adipose tissue of mice fed a high-fat diet. *Am J Physiol Endocrinol Metab* 2021;321:E560-E70.
- [17] Kuo CS, Chen JS, Lin LY, Schmid-Schonbein GW, Chien S, Huang PH, et al. Inhibition of serine protease activity protects against high fat diet-induced inflammation and insulin resistance. *Sci Rep* 2020;10:1725.
- [18] Rapohn I, Elias I, Weiner J, Pujol A, Kehr S, Chad A, et al. Overexpressing high levels of human vaspin limits high fat diet-induced obesity and enhances energy expenditure in a transgenic mouse. *Front Endocrinol (Lausanne)* 2023;14:1146454.
- [19] Nakatsuka A, Wada J, Iseda I, Teshigawara S, Higashio K, Murakami K, et al. Vaspin is an adipokine ameliorating ER stress in obesity as a ligand for cell-surface GRP78/MJ1-1 complex. *Diabetes* 2012;61:2823–32.
- [20] Liu P, Li G, Wu J, Zhou X, Wang L, Han W, et al. Vaspin promotes 3T3-L1 preadipocyte differentiation. *Exp Biol Med (Maywood)* 2015;240:1520–7.
- [21] Zieger K, Weiner J, Krause K, Schwarz M, Kohn M, Stumvoll M, et al. Vaspin suppresses cytokine-induced inflammation in 3T3-L1 adipocytes via inhibition of NFkappaB pathway. *Mol Cell Endocrinol* 2018;460:181–8.
- [22] Heiker JT, Kloting N, Kovacs P, Kuettner EB, Strater N, Schultz S, et al. Vaspin inhibits kallikrein 7 by serpin mechanism. *Kell Mol Life Sci* 2013;70:2569–83.
- [23] Fischer J, Meyer-Hoffert U. Regulation of kallikrein-related peptidases in the skin - from physiology to diseases to therapeutic options. *Thromb Haemost* 2013;110:442–9.
- [24] McGovern JA, Meinert C, de Veer SJ, Hollier BG, Parker TJ, Upton Z. Attenuated kallikrein-related peptidase activity disrupts desquamation and leads to stratum corneum thickening in human skin equivalent models. *Br J Dermatol* 2017;176:145–58.

- [25] Furio L, Hovnanian A. Netherton syndrome: defective kallikrein inhibition in the skin leads to skin inflammation and allergy. *Biol Chem* 2014;395:945–58.
- [26] Di Paolo CT, Diamandis EP, Prassas I. The role of kallikreins in inflammatory skin disorders and their potential as therapeutic targets. *Crit Rev Clin Lab Sci* 2021;58:1–16.
- [27] Guo CJ, Mack MR, Oetjen LK, Trier AM, Council ML, Pavel AB, et al. Kallikrein 7 promotes atopic dermatitis-associated itch independently of skin inflammation. *J Invest Dermatol* 2020;140(1244–52):e4.
- [28] Kasperek P, Ileninova Z, Zbodakova O, Kanchev I, Benada O, Chalupsky K, et al. KLK5 and KLK7 ablation fully rescues lethality of Netherton syndrome-like phenotype. *PLoS Genet* 2017;13:e1006566.
- [29] Xiang F, Wang Y, Cao C, Li Q, Deng H, Zheng J, et al. The Role of Kallikrein 7 in Tumorigenesis. *Curr Med Chem* 2022;29:2617–31.
- [30] Kunath A, Weiner J, Krause K, Rehders M, Pejkovska A, Gericke M, et al. Role of kallikrein 7 in body weight and fat mass regulation. *Biomedicines* 2021:9.
- [31] Zieger K, Weiner J, Kunath A, Gericke M, Krause K, Kern M, et al. Ablation of kallikrein 7 (KLK7) in adipose tissue ameliorates metabolic consequences of high fat diet-induced obesity by counteracting adipose tissue inflammation in vivo. *Cell Mol Life Sci* 2018;75:727–42.
- [32] Speakman JR, Fletcher Q, Vaanholt L. The ‘39 steps’: an algorithm for performing statistical analysis of data on energy intake and expenditure. *Dis Model Mech* 2013;6:293–301.
- [33] Virtanen KA. Adipose tissue: structure and function of brown adipose tissue. In: Caballero BFP, Toldrá F, editors. *Encyclopedia of food and health*. Oxford: Academic Press; 2016. p. 30–4.
- [34] Galarraga M, Champion J, Munoz-Barrutia A, Boque N, Moreno H, Martinez JA, et al. Adiposoft: automated software for the analysis of white adipose tissue cellularity in histological sections. *J Lipid Res* 2012;53:2791–6.
- [35] Pineda-Torra I, Gage M, de Juan A, Pello OM. Isolation, culture, and polarization of murine bone marrow-derived and peritoneal macrophages. *Methods Mol Biol* 2015;1339:101–9.
- [36] Braune J, Lindhorst A, Froba J, Hobusch C, Kovacs P, Blüher M, et al. Multinucleated giant cells in adipose tissue are specialized in adipocyte degradation. *Diabetes* 2021;70:538–48.
- [37] Christen L, Broghammer H, Rapohn I, Mohlis K, Strehlau C, Ribas-Latre A, et al. Myoglobin-mediated lipid shuttling increases adrenergic activation of brown and white adipocyte metabolism and is as a marker of thermogenic adipocytes in humans. *Clin Transl Med* 2022;12:e1108.
- [38] Szulcek R, Bogaard HJ, van Nieuw Amerongen GP. Electric cell-substrate impedance sensing for the quantification of endothelial proliferation, barrier function, and motility. *J Vis Exp* 2014;85:e51300.
- [39] American Diabetes Association Professional Practice C. 2. Classification and diagnosis of diabetes: standards of medical care in diabetes-2022. *Diabetes Care* 2022;45:S17–38.
- [40] Langhardt J, Flehmig G, Kloting N, Lehmann S, Ebert T, Kern M, et al. Effects of weight loss on glutathione peroxidase 3 serum concentrations and adipose tissue expression in human obesity. *Obes Facts* 2018;11:475–90.
- [41] Mardinoglu A, Heiker JT, Gartner D, Bjornson E, Schon MR, Flehmig G, et al. Extensive weight loss reveals distinct gene expression changes in human subcutaneous and visceral adipose tissue. *Sci Rep* 2015;5:14841.
- [42] Kloting N, Fasshauer M, Dietrich A, Kovacs P, Schon MR, Kern M, et al. Insulin-sensitive obesity. *Am J Physiol Endocrinol Metab* 2010;299:E506–15.
- [43] Saalbach A, Anderegg U, Wendt R, Beige J, Bachmann A, Kloting N, et al. Antifibrotic soluble Thy-1 correlates with renal dysfunction in chronic kidney disease. *Int J Mol Sci* 2023;24.
- [44] Schurfeld R, Sandner B, Hoffmann A, Kloting N, Baratashvili E, Nowicki M, et al. Renal function is a major predictor of circulating acyl-CoA-binding protein/diazepam-binding inhibitor. *Front Endocrinol (Lausanne)* 2023;14:1152444.
- [45] Song Y, Milon B, Ott S, Zhao X, Sadzewicz L, Shetty A, et al. A comparative analysis of library prep approaches for sequencing low input transcriptome samples. *BMC Genomics* 2018;19:696.
- [46] Picelli S, Faridani OR, Bjorklund AK, Winberg G, Sagasser S, Sandberg R. Full-length RNA-seq from single cells using Smart-seq2. *Nat Protoc* 2014;9:171–81.
- [47] Chen S, Zhou Y, Chen Y, Gu J. fastp: an ultra-fast all-in-one FASTQ preprocessor. *Bioinformatics* 2018;34: i884–i90.
- [48] Frankish A, Diekhans M, Ferreira AM, Johnson R, Jungreis L, Loveland J, et al. GENCODE reference annotation for the human and mouse genomes. *Nucleic Acids Res* 2019;47: D766–D73.
- [49] Bray NL, Pimentel H, Melsted P, Pachter L. Near-optimal probabilistic RNA-seq quantification. *Nat Biotechnol* 2016;34:525–7.
- [50] Robinson MD, Oshlack A. A scaling normalization method for differential expression analysis of RNA-seq data. *Genome Biol* 2010;11:R25.
- [51] Ritchie ME, Phipson B, Wu D, Hu Y, Law CW, Shi W, et al. limma powers differential expression analyses for RNA-sequencing and microarray studies. *Nucleic Acids Res* 2015;43:e47.
- [52] Kanehisa M, Goto S. KEGG: Kyoto encyclopedia of genes and genomes. *Nucleic Acids Res* 2000;28:27–30.
- [53] Subramanian A, Tamayo P, Mootha VK, Mukherjee S, Ebert BL, Gillette MA, et al. Gene set enrichment analysis: a knowledge-based approach for interpreting genome-wide expression profiles. *Proc Natl Acad Sci USA* 2005;102:15545–50.
- [54] Miller HE, Bishop AJR. Correlation AnalyzeR: functional predictions from gene co-expression correlations. *BMC Bioinformatics* 2021;22:206.
- [55] Emont MP, Jacobs C, Essene AL, Pant D, Tenen D, Colletuori G, et al. A single-cell atlas of human and mouse white adipose tissue. *Nature* 2022;603:926–33.
- [56] Herrero-Cervera A, Vinue A, Burks DJ, Gonzalez-Navarro H. Genetic inactivation of the LIGHT (TNFSF14) cytokine in mice restores glucose homeostasis and diminishes hepatic steatosis. *Diabetologia* 2019;62:2143–57.
- [57] Kim HM, Jeong CS, Choi HS, Kawada T, Yu R. LIGHT/TNFSF14 enhances adipose tissue inflammatory responses through its interaction with HVEM. *FEBS Lett* 2011;585:579–84.
- [58] Darimont C, Avanti O, Blancher F, Wagniere S, Mansourian R, Zbinden I, et al. Contribution of mesothelial cells in the expression of inflammatory-related factors in omental adipose tissue of obese subjects. *Int J Obes* 2008;32:112–20.
- [59] Reinisch I, Ghosh A, Noe F, Sun W, Dong H, Leary P, et al. Unveiling adipose populations linked to metabolic health in obesity. *Cell Metab* 2024;37:640–55.
- [60] Jablonski KA, Amici SA, Webb LM, Ruiz-Rosado Jde D, Popovich PG, Partida-Sanchez S, et al. Novel markers to delineate murine M1 and M2 macrophages. *PLoS One* 2015;10:e0145342.
- [61] Jaitin DA, Adlung L, Thaiss CA, Weiner A, Li B, Descamps H, et al. Lipid-associated macrophages control metabolic homeostasis in a Trem2-dependent manner. *Cell* 2019;178: 686–98 e14.
- [62] Nylander-Lundqvist E, Egelrud T. Formation of active IL-1 beta from pro-IL-1 beta catalyzed by stratum corneum chymotryptic enzyme in vitro. *Acta Derm Venereol* 1997;77:203–6.
- [63] Schultz S, Saalbach A, Heiker JT, Meier R, Zellmann T, Simon JC, et al. Proteolytic activation of prochemerin by kallikrein 7 breaks an ionic linkage and results in C-terminal rearrangement. *Biochem J* 2013;452:271–80.
- [64] Yu Y, Prassas I, Dimitromanolakis A, Diamandis EP. Novel biological substrates of human kallikrein 7 identified through degradomics. *J Biol Chem* 2015;290: 17762–75.
- [65] Russo L, Lumeng CN. Properties and functions of adipose tissue macrophages in obesity. *Immunology* 2018;155:407–17.
- [66] Johnson SK, Ramani VC, Hennings L, Haun RS. Kallikrein 7 enhances pancreatic cancer cell invasion by shedding E-cadherin. *Cancer* 2007;109:1811–20.
- [67] Ramani VC, Haun RS. The extracellular matrix protein fibronectin is a substrate for kallikrein 7. *Biochem Biophys Res Commun* 2008;369:1169–73.
- [68] Kyriakopoulou LG, Yousef GM, Scorilas A, Katsaros D, Massobrio M, Fracchioli S, et al. Prognostic value of quantitatively assessed KLK7 expression in ovarian cancer. *Clin Biochem* 2003;36:135–43.
- [69] Talieri M, Diamandis EP, Gourgoutis D, Mathioudaki K, Scorilas A. Expression analysis of the human kallikrein 7 (KLK7) in breast tumors: a new potential biomarker for prognosis of breast carcinoma. *Thromb Haemostasis* 2004;91:180–6.
- [70] Iakovlev V, Siegel ER, Tsao MS, Haun RS. Expression of kallikrein-related peptidase 7 predicts poor prognosis in patients with unresectable pancreatic ductal adenocarcinoma. *Cancer Epidemiol Biomarkers Prev* 2012;21:1135–42.
- [71] Ny A, Egelrud T. Transgenic mice over-expressing a serine protease in the skin: evidence of interferon gamma-independent MHC II expression by epidermal keratinocytes. *Acta Derm Venereol* 2003;83:322–7.
- [72] Gratchev A, Guillot P, Hakiy N, Politz O, Orfanos CE, Schledzewski K, et al. Alternatively activated macrophages differentially express fibronectin and its splice variants and the extracellular matrix protein beta1G-H3. *Scand J Immunol* 2001;53:386–92.
- [73] Alitalo K, Hovi T, Vaheri A. Fibronectin is produced by human macrophages. *J Exp Med* 1980;151:602–13.
- [74] Wallner K, Li C, Shah PK, Fishbein MC, Forrester JS, Kaul S, et al. Tenascin-C is expressed in macrophage-rich human coronary atherosclerotic plaque. *Circulation* 1999;99:1284–9.
- [75] Abbadi D, Laroumanie F, Bizou M, Pozzo J, Daviaud D, Delage C, et al. Local production of tenascin-C acts as a trigger for monocyte/macrophage recruitment that provokes cardiac dysfunction. *Cardiovasc Res* 2018;114:123–37.
- [76] Catalan V, Gomez-Ambrosi J, Rodriguez A, Ramirez B, Rotellar F, Valenti V, et al. Increased tenascin C and Toll-like receptor 4 levels in visceral adipose tissue as a link between inflammation and extracellular matrix remodeling in obesity. *J Clin Endocrinol Metab* 2012;97:E1880–9.
- [77] Fan N, Sun H, Wang Y, Zhang L, Xia Z, Peng L, et al. Midkine, a potential link between obesity and insulin resistance. *PLoS One* 2014;9:e88299.
- [78] Wu Y, Wu C, Shi T, Cai Q, Wang T, Xiong Y, et al. FAP expression in adipose tissue macrophages promotes obesity and metabolic inflammation. *Proc Natl Acad Sci USA* 2023;120:e2303075120.
- [79] Chen QY, Luo D, Seabra GM, Luesch H. Ahp-Cyclodepsipeptides as tunable inhibitors of human neutrophil elastase and kallikrein 7: Total synthesis of tutilamide A, serine protease selectivity profile and comparison with lnygbystatin 7. *Bioorg Med Chem* 2020;28:115756.
- [80] Murafuji H, Sugawara H, Goto M, Oyama Y, Sakai H, Imajo S, et al. Structure-based drug design to overcome species differences in kallikrein 7 inhibition of 1,3,6-trisubstituted 1,4-diazepan-7-ones. *Bioorg Med Chem* 2018;26:3639–53.
- [81] Proost P, De Wolf-Peeters C, Conings R, Opendakker G, Billiau A, Van Damme J. Identification of a novel granulocyte chemotactic protein (GCP-2) from human tumor cells. In vitro and in vivo comparison with natural forms of GRO, IP-10, and IL-8. *J Immunol* 1993;150:1000–10.
- [82] Elgazar-Carmon V, Rudich A, Hadad N, Levy R. Neutrophils transiently infiltrate intra-abdominal fat early in the course of high-fat feeding. *J Lipid Res* 2008;49: 1894–903.
- [83] Wood IS, Wang B, Jenkins JR, Trayhurn P. The pro-inflammatory cytokine IL-18 is expressed in human adipose tissue and strongly upregulated by TNFalpha in human adipocytes. *Biochem Biophys Res Commun* 2005;337:422–9.
- [84] Ahmad R, Thomas R, Kochumon S, Sindhu S. Increased adipose tissue expression of IL-18R and its ligand IL-18 associates with inflammation and insulin resistance in obesity. *Immun Inflamm Dis* 2017;5:318–35.

- [85] Peeraully MR, Jenkins JR, Trayhurn P. NGF gene expression and secretion in white adipose tissue: regulation in 3T3-L1 adipocytes by hormones and inflammatory cytokines. *Am J Physiol Endocrinol Metab* 2004;287:E331–9.
- [86] Halvorsen B, Santilli F, Scholz H, Sahraoui A, Gulseth HL, Wium C, et al. LIGHT/TNFSF14 is increased in patients with type 2 diabetes mellitus and promotes islet cell dysfunction and endothelial cell inflammation in vitro. *Diabetologia* 2016;59:2134–44.
- [87] Bassols J, Moreno-Navarrete JM, Ortega F, Ricart W, Fernandez-Real JM. LIGHT is associated with hypertriglyceridemia in obese subjects and increased cytokine secretion from cultured human adipocytes. *Int J Obes* 2010;34:146–56.
- [88] Ghodse SV, Lazarus RA. Analysis of kallikrein-related peptidase 7 (KLK7) autolysis reveals novel protease and cytokine substrates. *Biol Chem* 2024. <https://doi.org/10.1515/hsz-2024-0127>.